Development of gallium-oxide (Ga2O3) coatings by non-aqueous sol-gel routes for electronic applications

Author:
Mohammadali, Saeed

Publication Date:
2013

DOI:
https://doi.org/10.26190/unsworks/16369

The University of New South Wales

Faculty of Science

School of Materials Science and Engineering

Development of Gallium-oxide (Ga_2O_3) Coatings by Non-Aqueous Sol-Gel Routes for Electronic Applications

A Thesis

By

Saeed Mohammadali

Submitted in Partial Fulfilment of the

Requirements for the Degree

Of

Master of Engineering

In

Materials Science and Engineering

March 2013

CERTIFICATE OF ORIGINALITY

I hereby declare that this submission is my own work and to the best of my knowledge it contains no materials previously published or written by another person, nor material that to a substantial extent has been excepted for the award of any other degree or diploma at UNSW or any other educational institution, except where due acknowledgement is made in the thesis. Any contribution made to the research by other, with whom I have worked at UNSW or elsewhere, is explicitly acknowledged in the thesis.

I also declared that the intellectual content of this thesis is the product my own work, except to the extent that assistance from others in the project's design and conception or in style, presentation and linguistic expression is acknowledged.

(Signed)..... Saeed Mahdi .....

ACKNOWLEDGEMENTS

There are many people contributed to this work, whilst it would be impossible to mention them all here, I offer my sincere thanks to all of them. There are, however, those who have been particularly influential and I wish to recognise.

My supervisor, Dr. Owen Standard, has provided incredible support throughout the period of this research and he has dedicated generous amount of his time and knowledge. I cannot thank him enough for his patience and enthusiasm to further my knowledge and understanding.

I would also like to thank Professor Chris Sorrell for his valuable advice and for helpful discussions I had with him.

I wish to thank Professor Sean Li and his academic group who helped me with the modelling part of my project. Especial thanks go to Dr. Mohammad H.N. Assadi, Professor Li's postdoctoral fellow, for the hours spend helping me learn Materials Studio, the modelling software.

Thanks to all members of staff in the School of Materials Science and Engineering, UNSW, from technical to academic and administrative, for making the course of this master incredibly enjoyable. Many thanks to all my friends at UNSW for their kind help and support.

I have been fortunate to receive much support from my family, which has played a large role in the completion of this project. I wish to thank my parents for their support throughout my study. Finally, I wish to express my special gratitude to my wife, Tina, for her endless love, encouragement and incredible patience during my research.

ABSTRACT

The overall aim of this thesis was to develop a sol-gel gallium oxide (Ga_2O_3) coating and to study the phase evolution in coating, and to evaluate theoretically the crystal structure and electrical properties of coating by modelling the intrinsic- and doped-Ga_2O_3 structure using Materials Studio software, and to solid theoretical result, experimental work was performed and compared with the simulation results.

The most stable phase of gallium oxide (β-Ga_2O_3) is a wide band gap (4.9eV) metal oxide having a wider range of important applications. β-Ga_2O_3 is thermally and chemically stable at high temperatures and so exhibits very stable operating characteristics over large temperature ranges.

The major limitations of this coating arise from it having high resistivity. Monoclinic gallium oxide (β-Ga_2O_3) is one of the most promising materials for the device applications because of its wide band gap which gives high transparency from the visible into the UV wavelength regions (~260 nm). However, the high electrical resistivity of Ga_2O_3 coatings is going to be a significant issue making limitation for this coating to be used in optoelectronic devices. Therefore, incorporation of dopants to reduce Ga_2O_3 resistivity is desirable.

To develop Ga_2O_3 coating, two types of sols were prepared in this work using gallium isopropoxide as the starting precursor. The first sol (Type-I sol) was prepared via an aqueous route based on the method developed by Yoldas for alumina sol-gel coatings. The other sol (Type-II sol) was prepared via a non-aqueous route involving 2-methoxyethanol (MOE) as the solvent. The principle of coating process

was the deposition of these sols onto substrate (glass and quartz) by spin coating followed by drying and then heat treating at elevated temperature. The Type-I sol did not gelate during the deposition process as evidenced by the lack of any visible coating on the substrates. In contrast, the Type-II sol produced obvious coatings, albeit with varying extent of cracking depending on the deposition and heat-treatment conditions.

In another stage of project, the effects of the coating thickness, heat treatment conditions, and substrate type on coating structural evolution were investigated. Phase composition in the Ga_2O_3 sol-gel coating was studied as function of heat-treatment conditions. The initial deposited phase of gallium oxide transformed to α-Ga_2O_3 and then to β-Ga_2O_3 with increasing temperature. At 500°C, α-Ga_2O_3 phase started to form and upon heating at 900°C, β-Ga_2O_3 was only stable phase of gallium oxide. Subsequent heat treatment at different heating temperature for 2 h affected the coating behaviour in terms of the amount of cracking. The amount of cracking tended to increase with increasing heating rate and with increasing coating thickness. The choice of substrates for Ga_2O_3 was studied since it is critical and substantial for making high-quality coatings.

In this work, the effect of adding different dopants on the electrical properties of gallium oxide coatings were investigated theoretically using software called Materials Studio. The Modeling of Ga_2O_3 showed that the introduction of the Sn and Zn caused the impurity energy level at the bottom of the conduction band. Therefore, the conductivity of the Zn-doped and Sn-doped β-Ga_2O_3 was improved compared to the intrinsic β-Ga_2O_3.

In order to assess the simulation result and obtain how much the results are close to the practical results, experimental work was carried out by measuring the bandgap of pure β-Ga_2O_3, Zn3%-doped Ga_2O_3, and Zn6%-doped Ga_2O_3. The study indicated that in spite of a deviation in values between the experiment and simulation, the values were considered fit well, and there was a consistency between simulation and experiment results.

It was found that the experimental value of the bandgap energy for pure β-Ga_2O_3 agreed reasonably well with values reported in the literature and the experimental values for the pure and doped coatings were consistently ~2 times higher than the simulated values which suggested that the structural model used to calculate the bandgap energies systematically underestimated the values. This was attributed to limitations in the structural model. Regardless, the structural model was considered reliable for predicting the effects of dopants on selected structural and electronic properties of Ga_2O_3.

Table of Contents

LIST OF FIGURES

LIST OF TABLES

1. Introduction

1.1 AIMS OF RESEARCH PROJECT

The major aim of the research project was to develop a convenient and reliable sol-gel coating technique for the deposition of polycrystalline pure- and doped-gallium oxide (Ga_2O_3) on amorphous and crystalline substrates for optoelectronic applications. Parallel to this was the major aim to theoretically model the crystal structure and electrical properties of pure- and doped-Ga_2O_3 coatings to predict and understand the role of dopant cations in the semiconducting behaviour of Ga_2O_3. These aims were achieved by the completion of the following main areas of research: study of the gelation behaviour of pure- and doped-Ga_2O_3 coatings; study of the drying and firing shrinkage characteristics so as to minimise/eliminate cracking in coatings and to optimise coating quality; study of the microstructural and phase evolution within the coatings as a function of heat-treatment conditions

(temperature and time) and substrate type (glass versus quartz); elucidation the phase transformation mechanism in the coating for the conversion of the initial gallium-oxide precursor (sol) to β-Ga_2O_3 during heat treatment; modelling of the effect of divalent and/or tetravalent solid solution dopant cations (Sn, W, and Zn) on the crystal structure and electrical properties of Ga_2O_3 using proprietary software; and experimental measurement of the bandgap energy of pure β-Ga_2O_3 sol-gel coatings and coatings doped with a selected dopant (Zn) to enable comparison with theoretical values given by the structural model. The research project consisted of four main stages of experimental work as shown schematically in Fig. 1.1.

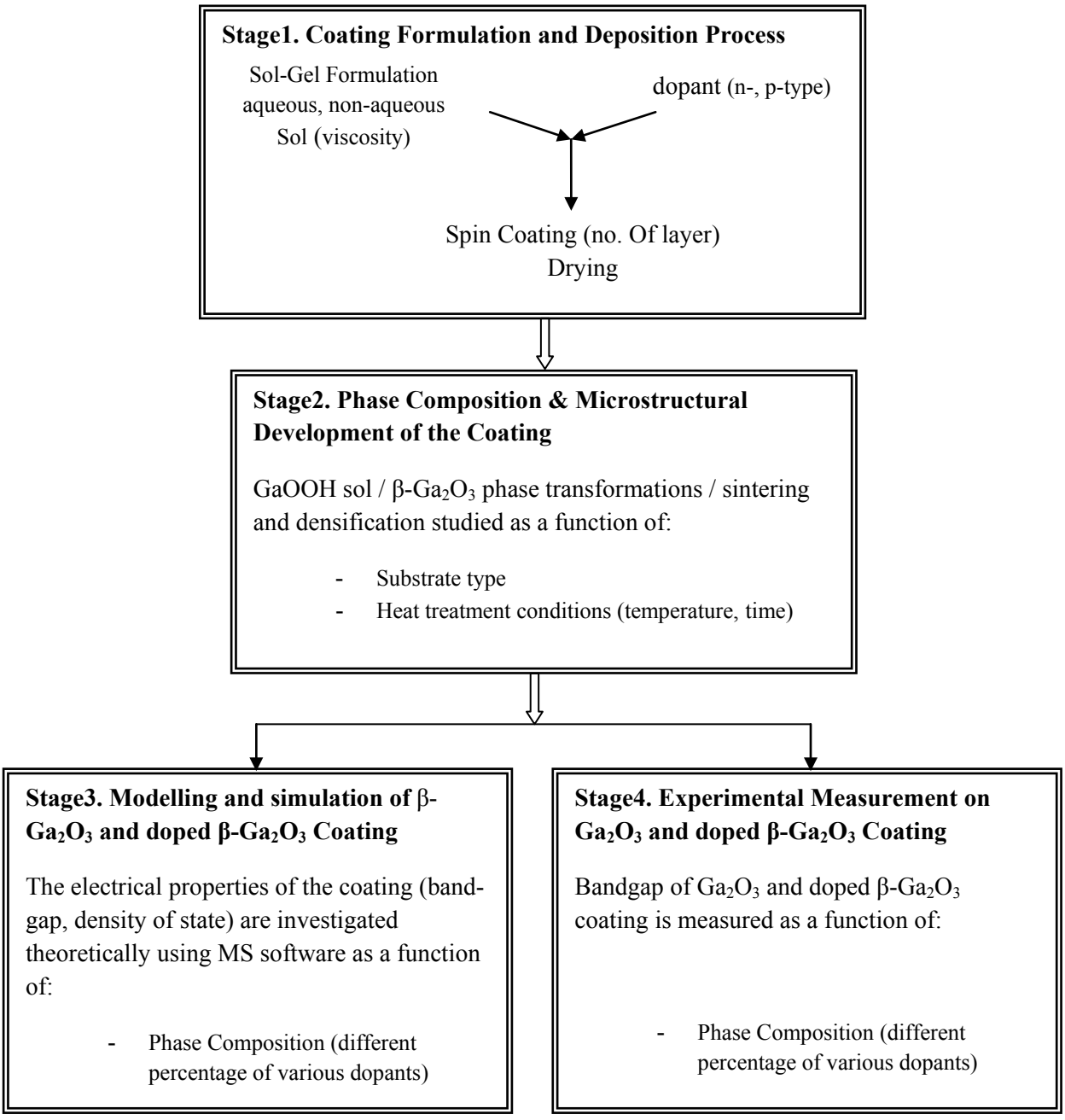

Fig.1.1 Main stages of experimental work

2. Literature Review

2.1 INTRODUCTION

In this section, applications, properties, and limitations of Ga_2O_3 coating will be discussed. Then various techniques to fabricate this type of coating are explained, mostly sol-gel process which is the main technique of this work are discussed. At the end of this section, the effect of substrates and dopants on the properties of Ga_2O_3 coatings fabricated by sol-gel technique is reviewed.

2.2 Ga_2O_3 COATING

2.2.1 Applications

The most stable phase of gallium oxide (β-Ga_2O_3) is a wide bandgap (4.9eV) metal oxide having a wide range of important applications including anti-reflection and passivation coatings [1], semiconducting lasers [2], solar cells [3], field-effect

devices [4], switching memories [5], and high-temperature gas sensors [6, 7]. β-Ga_2O_3 is thermally and chemically stable at high temperatures and so exhibits very stable operating characteristics over large temperature ranges. For example, β-Ga_2O_3 has a monoclinic crystal structure at room temperature and this structure is retained at all temperatures up to the melting point (~2000˚C). Furthermore, unlike other metal oxides, no surface reduction of the Ga_2O_3 occurs [8]. As a consequence of its high stability and wide bandgap value, it is a promising material for use in gas sensors at high temperatures and, for example, has used as a high-temperature (~800-1000°C) oxygen sensor [9, 10]. Since gas-sensing properties are expected to improve at lower crystallite sizes (due to an increased surface area), producing nanocrystalline to operate β-Ga_2O_3 in this temperature range is likely to be highly advantageous for this application. Also, β-Ga_2O_3 gas sensors have a short response time and a good sensitivity, which are desirable characteristics of a good gas sensor.

The interest in electronic and optical properties of β-Ga_2O_3 has recently increased because of its potential applications as an ultraviolet transparent conducting oxide [11]. Ga_2O_3-based glasses constitute an advanced class of optical glasses and have attracted interest as a phosphor material for applications in thin film electroluminescent displays because of its significant luminescence characteristics [12].

2.2.2 Polymorphs of Ga_2O_3

Roy and Osborn [13] reported five polymorphs of Ga_2O_3: α, β, γ, δ and ε phases. The occurrence and stability of the polymorphs are dependent on the conditions of

preparation. Structural data and bandgap values of the Ga_2O_3 polymorphs are given in Table 2.1.

Table 2.1 Crystal structures, lattice parameters, space groups, and bandgap of Ga_2O_3 polymorphs [14, 15]

Phase	Crystal system	Lattice Parameters	Density (g/cm^3)	Space group	Band-gap (eV)
α	Hexagonal	a= 0.498 nm c= 1.343 nm α= 120˚	5.88	R3c	2.4
β	Monoclinic	a = 1.2214 nm b = 0.3037 nm c = 0.5798 nm β = 103.83˚	6.44	C2/m	4.9
γ	Cubic spinel	a= 0.822 nm	–	Fd3m	–
δ	Body Centred Cubic	a= 0.952 nm	–	Ia3	2.3
ε	Orthorhombic	a = 5.12 nm b = 8.79 nm c = 9.41 nm	–	$Pna2_1$	–

β-Ga_2O_3 is reported to be the most stable form of gallium-oxide and hence the most common form of the oxide. Although other phases exist, they tend to convert to β-Ga_2O_3 upon heating above 870˚C [16-18]. The α-Ga_2O_3 structure is a low-temperature form below 600°C having a hexagonal crystal structure. The γ, δ phases are reported to have a cubic structure and bcc structure, respectively. The γ-phase is less clearly understood but it is known to show a spinel structure. ε-Ga_2O_3 was found to appear by heating δ-Ga_2O_3 at above 500˚C [5]. Yoshioka *et al.* [19] calculated Helmholtz free energies of formation as a function of temperature for the various phases of Ga_2O_3 (see Fig. 2.1) and determined that the formation energies are in the sequence β < ε < α < δ < γ at temperatures below 1400 K.

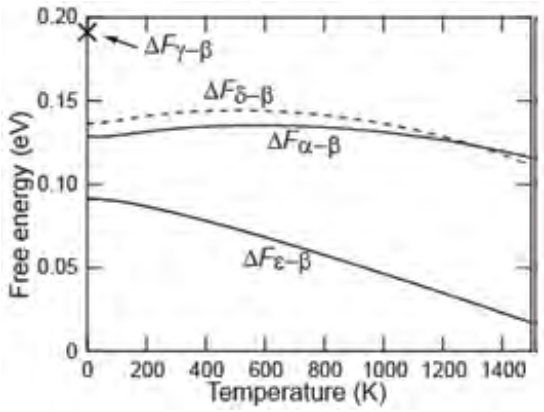

Fig. 2. 1 Temperature dependence of the differences in Helmholtz free energy between β- and other phases (α-, ε-, δ-, γ-) [8]

The thermodynamic stability of the various Ga_2O_3 polymorphs is reflected in their volume expansion characteristics in that, over the temperature range of ~298-1000 K, the values of the coefficient of thermal expansion increase in the order of β, ε, α, and δ (as shown in Fig. 2.2(a)). A similar trend exists below 400K Bulk moduli for the four phases are shown in plot 2(b). As can be noted, the calculated moduli increase in the order β, ε, δ, and α below 400K (127˚C).

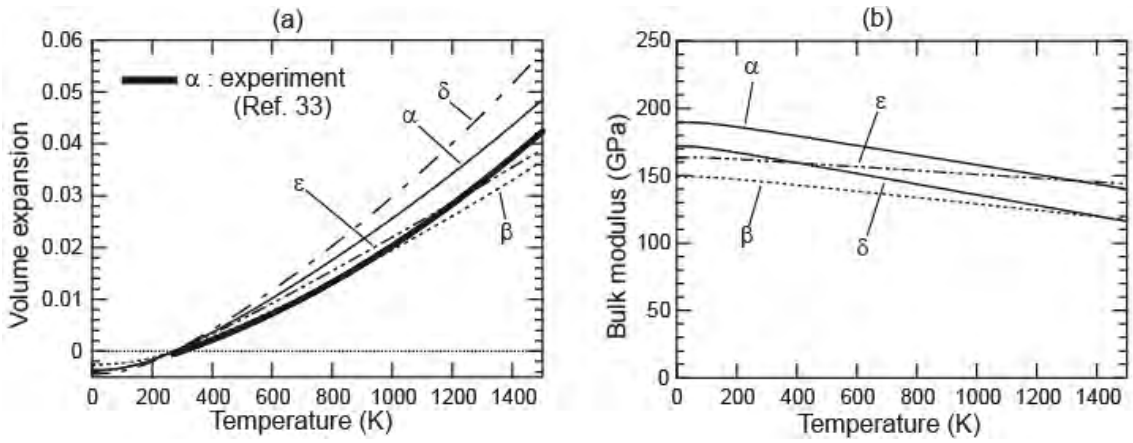

Fig. 2.2 Temperature dependence of volume expansion (a) and bulk modulus (b) for α-, β-, δ- and ε-Ga_2O_3 [8]

From these plots, the relative stability for the five phases can be shown. According to this calculation, the β- phase is energetically the most stable phase at temperatures below 1500K (1227˚C) and the ε-phase is more stable than the δ-phase at temperatures below 1600K (1327˚C) [19].

2.2.3 Limitations

In terms of Ga_2O_3 coating applications, the major limitations of this coating arise from it having high resistivity. β-type monoclinic gallium oxide (β-Ga_2O_3) is one of the most promising materials for the device applications because of its wide bandgap (E_g= 4.9 eV) which gives high transparency from the visible into the UV wavelength regions (~260 nm). However, the electrical resistivity of Ga_2O_3 coatings are high which would be a problem for these coatings to be considered as optoelectronic devices operated at short wavelengths. Therefore, finding a way to reduce Ga_2O_3 resistivity is desirable.

2.3 CERAMIC COATING TECHNIQUES

The objective is to deposit a ceramic layer on a substrate (metal, ceramic, polymer) to produce a surface having properties different to the bulk material. The applications of coatings are numerous and include tribology, heat insulation, corrosion resistance, electronics, optics, optoelectronic, biomedical, etc. Typically, the thickness of the layer various from a few atomic layers produced by vacuum deposition techniques up to a few millimeters.

Numerous techniques have been employed in the synthesis of gallium-oxide coatings including sputtering [20], chemical vapour deposition (CVD) [21], pulsed laser deposition (PLD) [22], solvent evaporation [23], molecular beam epitaxy (MBE) [24], spray pyrolysis [25], and sol-gel deposition [10, 26-28]. These techniques are examined next.

2.3.1 Vacuum Deposition

A large variety of ceramics can be deposited in vacuum (oxides, nitrides, carbides, and carbon-diamond) onto a similarly large variety of substrates. Vacuum deposition techniques can be classified into two main techniques: chemical vapor deposition (CVD) and physical vapor deposition (PVD) [21]. For both techniques, the formation of the thin coating can be broken down into three main stages (which can be separated or superimposed depending on the process) [21]. These three main stages that are important in the formation of the thin coating are as below: Production of the species to be deposited; transport of the species to the substrate; and deposition on the substrate and growth of the layer.

The two vacuum deposition techniques are examined separately below.

Chemical Vapour Deposition (CVD)

The technique consists of producing a layer, on a heated substrate, by chemical reaction starting from reactive species in the gas phase [29]. The reactive species can be discrete gases or generated from the decomposition of gas precursors. Typically, CVD deposited coatings are chemically homogenous and dense and have a good physical adhesion on the substrate.

The stages of process include substrate preparation, heating the substrate, substrate positioning and chemical deposition. To control the process, basic variables include temperature, pressure, and reactant activity. Reactions occur over a wide range of pressures and temperatures. Component on ranging from microsizes to macrosizes can be coated by CVD.

An important advantage of CVD methods is that they involve relatively low fabrication temperatures to produce coatings having high melting points that are otherwise difficult to fabricate by other methods because they require very high fabrication temperatures [29]. However, a major disadvantage is that the material deposition rate by CVD is very slow. The production of thick coatings and monolithic bodies can therefore be very time consuming and expensive. Another problem is the method produces microstructures consisting typically of fairly large grains which lead to low intergranular strength, poor electrical transport properties, and other diminished properties. Thus, CVD methods are limited mainly to the formation of thin films and coatings.

Physical Vapour Deposition (PVD)

PVD is a technique similar to CVD for coating materials in a vacuum but involves the transport of vapour without any chemical reactions [30]. The coating material is vaporised from the solid or liquid state with the resultant gaseous species being transported to the substrate where upon it condenses onto the surface by nucleation and growth. Vaporisation is performed by either evaporation or sputtering. The main evaporation methods are direct evaporation, reactive evaporation, and activated reactive evaporation. PVD coating process is performed in a vacuum chamber at a pressure of around 10^{-2} and 10^{-3} mbar. Advantages of PVD include the possibility to vary the substrate temperature; its versatility in composition of the deposit such as ceramic, pure metal or alloy; deposition of high purity coatings; and good bonding strength and excellent surface finish of coatings. Disadvantages of PVD processes include then being very costly and being capable of only short vapour diffusion distances.

Sputtering [25] is one of basic techniques of PVD. One advantage of this vapor phase technique is the versatility afforded by the possible use of multiple evaporation/sputtering sources, thereby providing considerable control over the coating composition and phase profile. However, vacuum conditions necessitate a confined space, which is not conducive to the cost effective handling of large area substrates. Sputtering techniques suitable for large area deposition require expensive vacuum equipment and sputtering targets.

2.3.2 Pulsed Laser Deposition (PLD)

Pulsed laser deposition (PLD) is a thin film deposition technique utilising a high power pulsed laser beam focused inside a vacuum chamber to strike a target of the material that is to be deposited [31]. This material is vaporized from the target which then deposits as a thin film on a substrate. This process can occur in ultra-high vacuum or in the presence of a background gas. For example, for the latter oxygen is commonly used when depositing oxides to ensure that the deposited coatings are fully oxygenated. While the principle and basic setup are simple and similar to other gas deposition techniques, the physical phenomena of laser-target interaction and coating growth are quite complex. The advantages of pulsed laser deposition are flexibility, fast response, energetic evaporants, and congruent evaporation. Disadvantages of this process are that small coating areas (limited uniformity), formation of particulates, and target surface modification [31].

2.3.3 Ion Implatation

Ion implantation is a popular technique to improve the wear resistance and corrosion resistance of materials. It is a process in which chosen atomic species are ionized and then accelerated in an electric field under a moderate vacuum and fired into the surface on the substrate. Coatings can be produced as thick as ~1 μm [32]. Process variables include ion dose, dose rate, substrate temperature, and annealing temperature. Ion implantation rates range between 10^{10} ion/cm^2 for semiconductor doping and 10^{19} ion/cm^2 for surface chemical conversion. Continuous or sequential processes of deposition and ion bombardment are possible by adaptation of the

implantation equipment. Advantages of ion implantation include: minimisation of thermal distortion of precision components by implantation at low temperatures; absence of an interface which eliminates de bonding due to mechanical stress or corrosion; and improvement of surface finish by sputtering erosion of the substrate. In addition, considerable biaxial compressive stress can induced in the surface layers and can even be used to close surface micro-cracks in ceramic materials [33]. Disadvantages of this process are that it requires expensive equipment and yields very low deposition rates.

2.3.4 Spray Pyrolysis

This technique involves heating a powder material to near its melting point to partially melt the particles and then accelerating the particles in a high velocity gas stream to project them against the substrate to be coated. Spray pyrolysis usually gives little significant heating of the substrate [12]. It is carried out in gas plasma, formed typically by ionizing a gas by arc discharging between a tungsten cathode and a copper anode. The initial gas used is an inert gas (argon or helium) and secondary gas may be added. The temperature in the centre of the plasma column exceeds 30 000˚C and this high temperature causes a rapid expansion of the gas thus producing the high velocity and high temperature spray gas stream needed for particle melting and deposition of the powder. Advantages of this coating technique include the ability to deposit thick coatings of uniform coverage at high deposition rates. However, the process is line of sight and coatings tend to have a higher amount of residual porosity as well as greater roughness compared with other techniques.

2.3.5 Sol-Gel Processing

Sol-gel processing is a type of colloidal processing route that is used to fabricate ceramic components in both bulk and coating forms [34]. A colloidal suspension may be defined as a dispersion of particles, each particle in the range of 1 to 1000 nm in at least one dimension, in a continuous liquid medium. Colloidal behaviour governed by the interactions between dispersed particles within the suspending medium. A distinguishing feature of such colloidal systems is the large interfacial area between the particles and the medium, and the development of surface charge on the particles, and these strongly influence characteristic particle-particle interactions such as agglomeration [35, 36].

Sol-gel coatings generally are thin films deposited on solid substrates from a liquid solution via the following steps: (a) preparation of the sol, (b) formation of coating layer on substrate, (c) drying the sol to a gel, and (d) firing of the coating layer on substrate. A sol is a dispersion of solid particles in a liquid phase where the particles are small enough (approximately 0.1-1 μm) to remain suspended. A gel is a solid containing a liquid component in an internal network structure so that both the liquid and solid are in highly dispersed state. In the gel state, material can be shaped into a useful product, e.g. bulk shape, coating, fibre, etc. In the sol-gel process, the precursors are starting compounds for preparation of a colloid consist of a metal surrounded by various ligands. These ligands are either organic compounds or inorganic salts such as alkoxide or nitride compound, respectively.

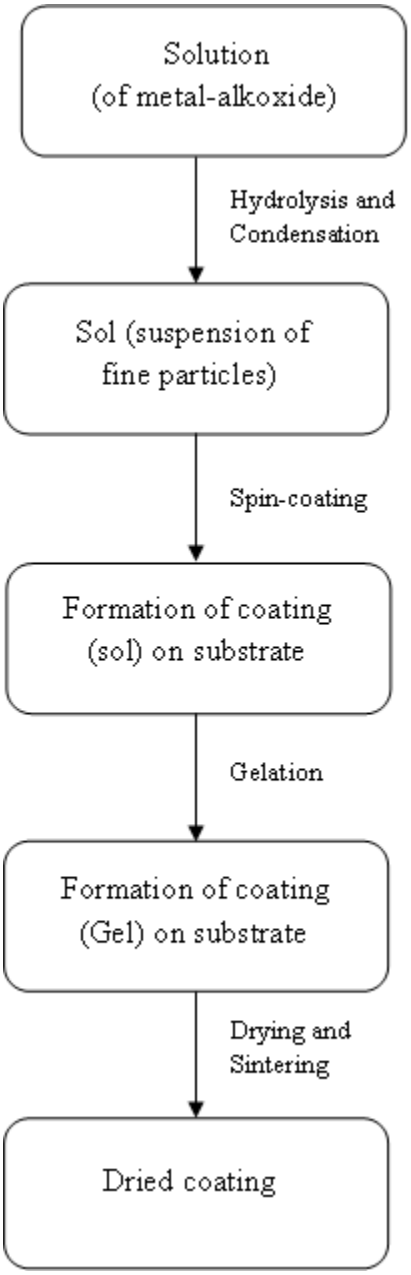

Fig. 2.3 Flow chart for sol-gel processing

Metal alkoxides are popular precursors because they react readily with water (solvent). The resultant solution is then hydrolysed to form a high-quality high-purity nano-cluster sol, and subsequently a gel [37]. Additives can also be added to control the viscosity and surface tension of the sol-gel to aid in the coating process. Colloidal dispersions (sols) are prepared by peptisation (with a mineral acid such as

HNO_3), while a gel is formed by dehydration or pH control. Sol-gel processing includes aqueous-based processes that start from a solution of metal salt and alcohol-based processes that derive from a metal alkoxide. In the aqueous-based process, sol formation is accomplished by hydrolysis of the metal ions, i.e. $M^{n+} + nH_2O \rightarrow M(OH)_n + nH^+$.

Gelation of the sol is accomplished by either the removal of water (dehydration gelation) or an increase in the pH (alkaline gelation). As water is removed during dehydration gelation, the energy barrier to gelation is reduced by the increase in electrolyte concentration in diffuse layer. In alkaline gelation, an increase in the pH reduces the magnitude of positive surface charge on the sol particles, which reduces the repulsive force between particles and lowers the height of the energy barrier. Compaction of the gelled coating during drying, as driven by capillary pressure, is resisted by aggregation due to gelation. Since colloidal (sol) particle compacts have very high surface energies, sintering can be done at temperatures well below required for the corresponding ceramic prepared by tradition powder compaction techniques. Formation of sol-gel coatings on substrates are performed by spin, dip, spray coating, or painting onto an appropriate substrate. The coated substrate is then fired to remove the water and organic material and to develop the final ceramic phase composition and microstructure in the coating [37, 38].

As indicated in flow chart (Fig. 2.3), the main sequence of steps in the solution sol–gel route has been outlined. The starting material normally consists of a solution of metal alkoxides in an appropriate solvent (water, alcohol, etc.). Metal alkoxides have the general formula $M(OR)_x$ and can be considered as either a derivative an alcohol,

ROH, where R is an alkyl group, in which the hydroxyl proton is replaced by a metal, M, or a derivative of a metal hydroxide, $M(OH)_x$. Under constant stirring at temperatures slightly above room temperature (normally 50 - 90°C) and with suitable concentration of reactants and pH of the solution, hydrolysis and condensation reactions may occur, leading to the formation of polymer chains.

For Gallium-aloxides, $Ga(OR)_3$, the reactions may be expressed as:

Hydrolysis: $Ga(OR)_3 + H_2O \rightarrow Ga(OR)_3 + ROH$

Condensation: $Ga(OR)_2(OH) + Ga(OR)_3 \rightarrow (RO)_2 \cdots M - O - M \cdots (OR)_2 + ROH$

Polymerization of the species formed by the hydrolysis and condensation reactions together with interlinking and cross-linking of the polymer chains eventually leads to a marked increase in the viscosity of the reaction mixture and the production of a gel. The gel has a continuous solid network and a finite shear modulus.

Drying: The remainder of the volume consists of liquid that must be removed prior to firing. Drying of the gels can be the most time consuming and difficult step in the overall fabrication route. Normally, the liquid is present in fine channels, typically 2-50 nm diameter. Removal of the liquid by evaporation has two main consequences: large capillary stresses are generated, and the gel undergoes considerable shrinkage under the action of the capillary stress. That is why there is a huge amount of crack after drying. Aging before drying helps to strengthen the gel network and thereby reduce the risk of fracture.

2.3.6 Comparison between Ceramic Coating Techniques

In this work, a sol-gel technique is utilised to make Ga_2O_3 coating. For oxides such as Ga_2O_3, the sol-gel process has several advantages over other fabrication methods including: it is a more convenient and cost effective process; it is easier to control the composition of the coating and to produce the coating with purity and superior uniformity; it permits coating of complex geometries of irregular-shaped components; and, it gives good control of microstructure; it involves lower preparation temperatures compared with other techniques [37]. Also, incorporation of dopants into coating formulations is simple and relatively large areas of substrates can be coated [39].

As an example shown in Table 2.2, Bae [40] evaluated ceramic coating prepared by various methods such as PVD, CVD, ion implantation, spray pyrolysis, and sol-gel in terms of bonding strength with substrate, coating hardness, surface roughness, thickness control, and cost. This evaluation suggested that the sol-gel technique is scored higher than the other methods.

Table 2.2 Evaluation of various ceramic coating methods for deposition of oxides [33]

Properties (Weighting)	PVD	CVD	Ion Implantation	Spray Pyrolysis	Sol-Gel
Bonding strength	****	****	*****	***	*****
Coating hardness	****	****	****	***	****
Surface roughness	*****	*****	*****	***	****
Thickness control	***	***	**	*****	**
Cost	***	****	**	****	*****
Evaluation	0.78	0.81	0.76	0.70	0.82

*:20%, **:40%, ***:60%, ****:80%, *****:100%

2.4 COLLOIDAL BEHAVIOUR

A colloid consists of two distinct phases: a continuous phase and a dispersed phase. The two phases may be solids, liquids, or gases, giving rise to various types of colloidal systems. The dispersed particles generally have dimensions ranging between 1 and 1000 nm [35]. In the processing of ceramics, colloidal suspensions (sols) consisting of a dispersion of solid particles in a liquid, are of particular interest. The size of the polymer molecules in solution falls in the colloidal size range so that these systems are considered part of colloid science. Colloidal behavior is the interaction between the dispersed particles and the suspending medium [36]. A distinguishing feature of a colloidal system is that the large interfacial area between the particles and the medium, and the development of surface charge on the particles, controls characteristic particle-particle interactions such as agglomeration or flocculation.

2.4.1 Stabilization of Colloidal Suspensions

A basic problem underlying sol-gel processing is the stability of colloidal suspensions. Obviously the particles should not be too large otherwise gravity will make sedimentation occur more quickly. Another important consideration is the attractive force between the particles. Attractive van der Waals forces exist between particles regardless of whether other forces are present. If the attractive force is large, the particles will collide and agglomerate together (flocculate) leading to rapid settling of the particle clusters [36]. Most techniques employed to prevent flocculation rely on the introduction of repulsive forces by repulsion between electrostatic charges (electrostatic stabilization), repulsion between polymer molecules (steric stabilization), or some combination of the two (electrosteric stabilization). A stable colloidal suspension may be consolidated into a densely packed structure; however, an unstable flocculated suspension may lead to a loosely packed structure or, under certain conditions, to a particulate gel with a relatively low density [36, 37]. The motion of the particles when subjected to an electric field (electrophoresis) can be a source of valuable information for determining the surface charge of the particles. Colloidal suspensions, especially concentrated suspensions, also have remarkable rheological properties. A good paint must flow easily when applied to the surface to be painted but then must become rigid enough to prevent it from flowing off a vertical surface. In ceramic processing, the rheological behavior of the suspension can be used as a direct process parameter to control and optimize the structure of the green body produced by the consolidation process [41].

2.4.2 Rheology of Colloidal Suspensions

The term *rheology* refers to the deformation and flow characteristics of matter. Rheological measurements monitor changes in flow behavior (strain) in response to an applied stress. Rheological measurements are widely used to characterize the properties of colloidal suspensions [36]. They can be used as a method of analysis as, for example, by measuring the viscosity of the suspension to determine the optimum concentration of dispersant required to stabilizing a suspension. Rheological measurements are also used commonly as a quality control technique to minimize the batch-to-batch variation of suspension properties prior to coating and consolidation. Furthermore, rheological measurements can be used as a direct processing parameter for the coating in that the suspension should have a low enough viscosity to enable it can to be cast into the desired shape [35, 36].

2.4.3 Effect of Solvents

A solvent can affect chemical reactivity with an effect on solubility and stability, and choosing the appropriate solvent allows for thermodynamic and kinetic control over a chemical reaction [42]. The process of dissolution depends upon the free energy change of both the solute and the solvent. The free energy of solvation is a combination of several factors. Firstly, a cavity must be created in the solvent. The creation of the cavity will be enthalpically and entropically unfavorable as the ordered structure of the solvent increases and there are fewer solvent-solvent interactions. Secondly, the solute must separate out from the bulk solute. This is enthalpically unfavorable as solute-solute interactions are breaking but is

entropically favorable [42,43]. Thirdly, the solute must occupy the cavity created in the solvent. This results in favorable solute-solvent interactions and is also favorable as the mixture is more disordered than when the solute and solvent are not mixed. Dissolution often occurs when the solute-solvent interactions are similar to the solvent-solvent interactions, signified by the term like dissolves like. Hence, polar solutes dissolve in polar solvents, whereas nonpolar solutes dissolve in nonpolar solvents. There is no one measure of solvent polarity and so classification of solvents based on polarity can be carried out using different scales. Different solvents can affect the equilibrium constant of a reaction and the equilibrium is shifted in the direction of the substance that is preferentially stabilized [44].

The chemical reactions involved in the sol-gel processing of Ga_2O_3 involves gallium isopropoxide as a solute and methoxyethanol (MOE) and/or water as the solvent. The ability of MOE or water to solvate whatever solvent species depends on their relative acidity/basicity (i.e., the ionization equilibrium of the solvent) as well as the magnitude of the polar charge of each of them relative to that of the solute. This can be considered in terms of the (relative) dielectric constants of the solute and solvent species. The relative dielectric constant of water (78 at 20°C [45]) is significantly greater than that of MOE (17.2 at 20°C [45]) which indicates that the water is the more polar species and therefore is the solvent which should give faster and more complete solvation of the polar gallium isopropoxide solute.

2.4.4 Essential Requirements for Ga_2O_3 Coatings

In general, a sol should be a homogeneous low-viscosity liquid without having tendency for sedimentation or phase separation. A sol that is potentially suitable for the formation of films or coatings should have the following general characteristics [27,46]: (1) thickness uniformity; (2) compositional homogeneity; (3) structural homogeneity; (4) ability to form crack-free coatings. In addition, sol gel coatings for electronic services in particular should be transparent in the visible light range [1].

The essential requirements of Ga_2O_3 coating for use in the electronic services more specifically in high-temperature applications include [9]: (1) being theoretically dense and free from any cracks and porosity; (2) being well-bonded to the substrate to prevent interfacial cracking and coating delamination in service; and (3) correct microstructure including phase composition, grain size, etc.

2.5 SOL-GEL PROCESSING OF Ga_2O_3

Ga_2O_3 sols can be prepared through two different routes based on either an aqueous solvent (Type-I) [38] or a non-aqueous solvent (Type-II) [46,47]. In both types, gallium isopropoxide (GaP) is used as the starting material (precursor). The main stages involved in the processing in each route are summarised in Fig. 2.4.

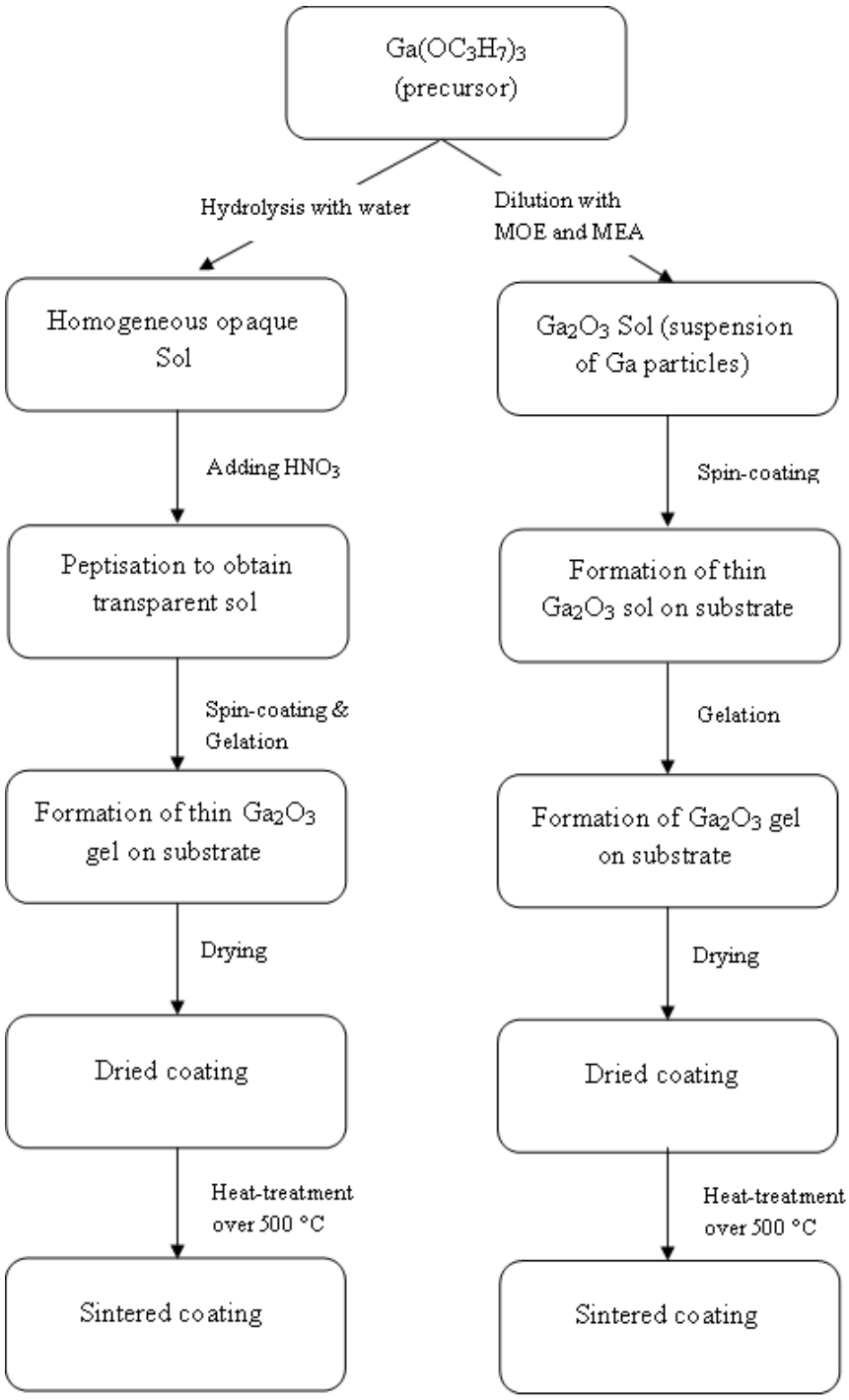

Fig. 2.4 Flow chart for sol-gel processing of Ga_2O_3

In Type-I, as a new technique based on Yoldas [38], GaP dissolved in the MOE is hydrolysed with water. This stage is done the same as Yoldas technique. The

solution is stirred for a while to obtain an opaque white solution. The pH of this solution is measured and adjusted to 2-3 by adding HNO_3, the same as Yoldas technique. This stage is called Peptisation and followed by stirring at temperature between 50-90°C for at least 1 h to become a transparent colloid solution. In this technique, the molar ratio of precursor, solvent, and acid is important and should be considered according to Yoldas technique [38].

In Type-II, 2-Methoxyethanol (MOE) and monoethanolamine (MEA) are used as the solvent and stabilizer, respectively. GaP is dissolved in a mixture of MOE and MEA at temperature between 50-90°C followed by stirring for 1 h to obtain a homogeneous and transparent solution [46,47].

These processes (Sol types I and II) are performed in a sealed flask immersed in a controlled-temperature silicon-oil bath. Then the sols are spin coated on the substrates and as indicated in Fig. 2.4 the gelation stage, drying, and sintering are done [38, 47].

2.5.1 Phase Evolution with Heat-Treatment

Depending on the particular chemical preparation route, gallium-oxide can exist in a variety of oxide and hydrated oxide forms [23]. Heat treatment of these phases converts them to the thermodynamically stable phase of β-Ga_2O_3 via one or more metastable transition phases including α-, γ-, δ-, and ε-Ga_2O_3. The sol-gel phase produced by the non-aqueous/aqueous routes from gallium alkoxide precursors is usually GaOOH [48,49]. The transition sequence from GaOOH via various metastable gallium oxide phases to β-Ga_2O_3 is shown in Fig. 2.5.

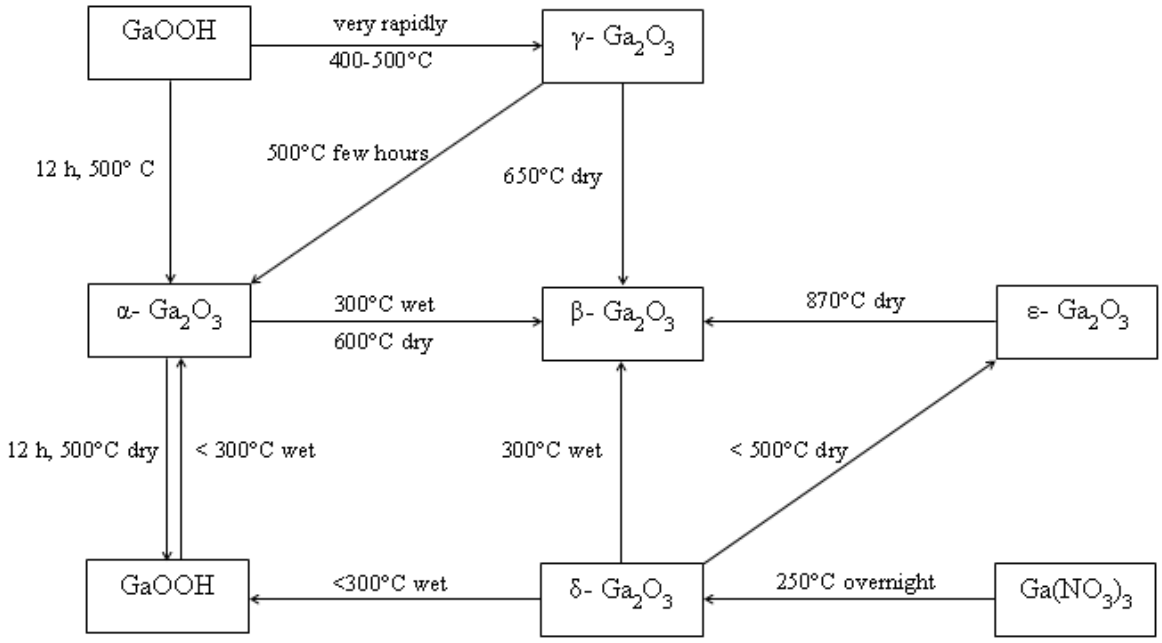

Fig. 2.5 Transformation relationships among the forms of Gallium oxide and its hydrates [13]

Roy and Osborn [13] reported that an $\alpha \rightarrow \beta$ transformation occurs at 300˚C under wet conditions and at 600˚C under dry conditions, $\varepsilon \rightarrow \beta$ transformation at 870˚C under dry atmosphere, and a $\delta \rightarrow \varepsilon$ transformation at above 500˚C under dry atmosphere (Fig. 2.5).

2.5.2 Effect of Substrate

The choice of substrates is critical and substantial for making high-quality coatings. Basic considerations include crystallographic lattice match, compatible thermal expansion, and solid-solubility between the coating and substrate. The lattice match between substrate and coating at the deposition temperature, as well as similarities in the crystal structure of substrate and coating, favor epitaxial coating growth [35, 36].

Usually, quartz and alumina have been considered as substrate for Ga_2O_3 coating, however from the relevant phase diagrams in Fig. 2.6, it can be seen that Al_2O_3 is a better choice for substrate than SiO_2. The reason is that beside of crystal structure similarity between Ga_2O_3 and Al_2O_3, they have a good solid-solution solubility in each other, which gives the possibility of forming a compositionally-graded inter-diffusion bond layer. It is considered that such a bond layer will give excellent coating adhesion though minimization of the stress discontinuity at the interface [50, 51].

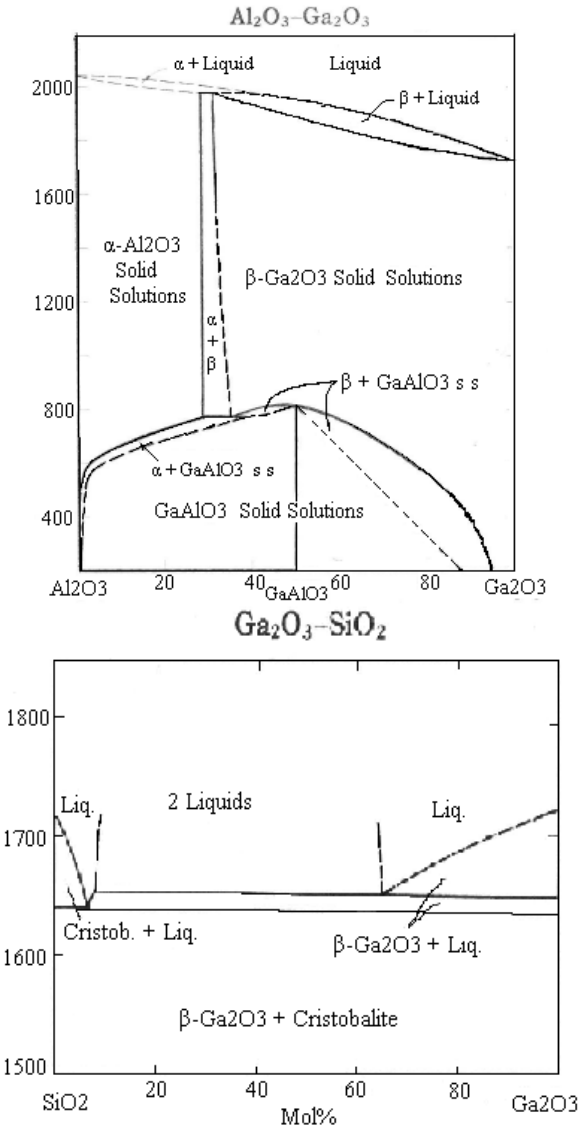

Fig. 2.6 Ga_2O_3-SiO_2 and Ga_2O_3-Al_2O_3 phase diagrams [50]

2.5.3 Inter-diffusion between Coating and Substrate

In the development of a ceramic coating, the heat treatment conditions (primarily temperature and time) are very important in that they affect the formation of the bond, densification and microstructural evolution of the coating, and the resultant properties of the substrate such as coating adhesion, strength, and surface roughness [36]. In the case of a Ga_2O_3 coating on an alumina substrate, an increase in temperature and heating time can affect the interface of coating and substrate by Al

diffusion into coating and Ga diffusion into substrate. Inter-diffusion between coating and substrate can be investigated by measuring the concentrations of Ga, Al, and O as a function of depth from the coating surface using X-ray photoelectron spectroscopy (XPS) [51]. In this work because the specific aim is the investigation of phase evolution in coating independent of substrate, this experiment is not run.

2.5.4 Incorporation of Dopants

In sol-gel technique, incorporation of dopants is easy and large area substrates can be coated readily [10]. However, the nature and content of dopants have a significant effect on the sol gel process. Doping may dramatically change the electrical properties of metal-oxide coatings. The resistivity of the Ga_2O_3 coatings can be tailored with different dopant and the concentrations. In addition, doping can affect the crystalline size. In this work, the effect of some dopants on gallium oxide coatings were investigated theoretically using software called Materials Studio. Also, to investigate which ions could be suitable as dopant for Ga^{3+} in terms of sol-gel process, doping solution of these ions with Ga^{3+} were made. Obviously, the reaction of compatible dopants with Ga^{3+} should lead to a homogenous solution.

In this work, to dope Ga_2O_3 sol with different concentration of dopants, the dopants which would be compatible with Ga_2O_3 were considered. In particular, an ionic / covalent radius of the dopant cation should be close to gallium, thus the dopant ions could go into the lattice as substitutional dopants. Based on this factor and from Pauling's ionic and covalent radii data, Sn^{4+}, Zn^{2+}, and W^{6+} ions were chosen as dopants for Ga^{3+}.

Electronegativity Role

Before studying the electrical properties of Ga_2O_3, a key factor which affects the electrical properties of metal oxides should be explained. This factor is electronegativity differences which drive charge transfers on molecule formation. In particular, in sol-gel technique which chemical reactions occur during the process, electronegativity is a significant factor which influences the electrical properties of resultant coating. It is the chemical potential of density functional theory. While energy and not electronegativity determines whether a chemical bond will form, electronegativity differences determine the charge transfers which occur on bond formation [36]. The method used for the preparation of a metal alkoxide depends, in general, on the electronegativity of the metal. The main methods may be divided into two groups: (1) reactions between metals and alcohols for the more electropositive metals (i.e., those with relatively low electronegativity values) and (2) reactions involving metal chlorides for the less electropositive metals or electronegative elements (i.e., those with relatively high electronegativity values).

The physical properties of metal alkoxides depend primarily on the characteristics of the metal (e.g., the electronegativity, valence, atomic radius, and coordination number) and secondarily on the characteristics of the alkyl group (e.g., the size and shape). Therefore, as discussed electronegativity of metal in metal alkoxide involving in the chemical reaction plays a big role and should be considered.

2.6 ELECTRICAL PROPERTIES OF METAL OXIDES

To evaluate electrical properties of metal oxides, conductivity should be considered. The degree of conductivity depends on the bandgap (E_g). The term "bandgap" refers to the energy difference between the top of the valence band (E_v) and the bottom of the conduction band (E_c) (in electron volts) [52]. It is an energy range in a solid where no electron states can exist. A schematic of the basic bandgap model is shown in Fig. 2.7. This is equivalent to the energy required to free an outer shell electron from its orbit about the nucleus to become a mobile charge carrier, able to move freely within the solid material. The bandgap is therefore a major factor determining the electrical conductivity of a solid [53].

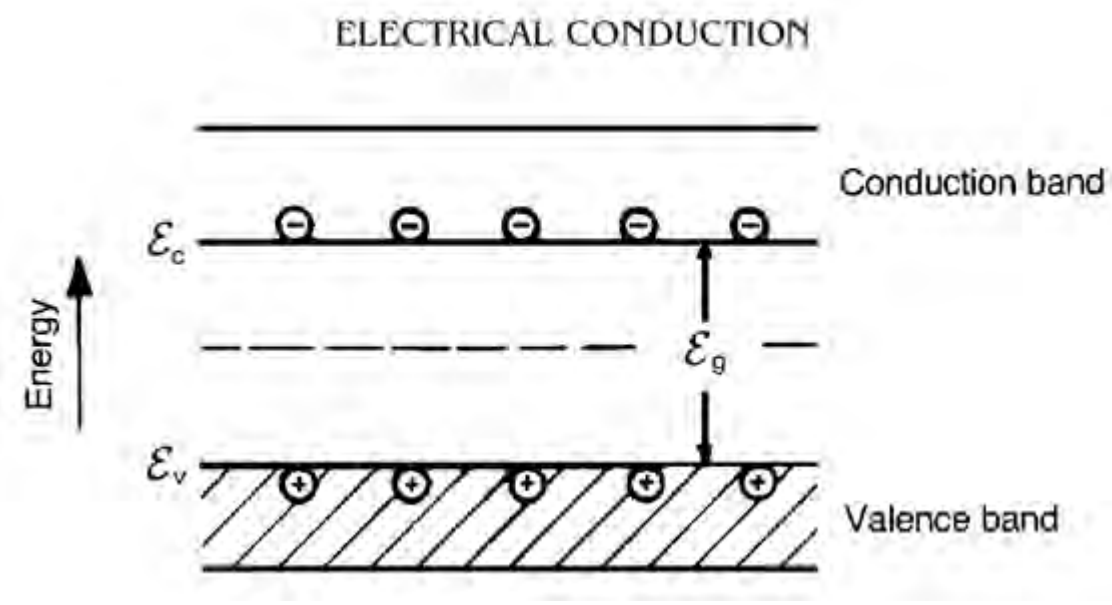

Fig. 2.7 Schematic of electrical conduction bands in materials [53]

Every solid has its own characteristic energy band structure and the variation in band structure is responsible for the wide range of electrical characteristics observed in various materials. In order for electrical charge to flow (i.e. current) in an oxide,

electrons must transfer from completely filled valence band levels across the bandgap and into the conduction band. This requires energy (work) to raise the energy potential of the electron from E_v to E_c. If the bandgap is large, upon applying an external electric field at room temperature, there will be only a few electrons that have the necessary energy to jump from the valence band to the conduction band. Increasingly temperature or supplying energy is thus required to provide enough energy to elevate sufficient numbers of electron into the conduction band to thus increase electrical conductivity [53, 54].

To improve the electrical properties of metal oxides, doping is intentionally used. Doping introduces impurities into extremely pure (also referred to as intrinsic) metal oxides for the purpose of modulating its electrical properties. The impurities are dependent upon the type of metal oxide [11]. To evaluate how dopants may affect electrical properties of metal oxides, the term 'Conductivity' should be studied.

2.6.1 Conductivity

Electrical conductivity (σ) is that property which relates the current density in a material to the electrical field impressed across it at steady state as follows [54]:

$$\sigma = \frac{1}{R} \times \frac{d}{A} \qquad (2-1)$$

where σ $(\Omega.m)^{-1}$ is the conductivity, A its area (m^2), d its thickness (m), and R its electrical resistance (Ω). The electrical conductivity is a measure of the charge-arraying ability of material given by $\sigma = nq\mu$ where

n = density of charge carriers (cm^{-3})

μ = mobility of charge carrier (cm^2/Vs)

q = charge (Coulombs, C)

The charge carriers may be either electrons (e^-) or holes (h°), or cations (M) and/or anions (X). Depending on which charge carriers predominate, the solid may be classified as primarily an electronic (n- or p-type) conductor or an ionic conductor. However, mixed conduction occurs and this conduction is then represented as [54]:

$$\sigma = \sigma_{electron} + \sigma_{ionic} \qquad (2-2)$$

Both types of conduction involve the presence of point defects in the crystal structure and these are examined next.

2.6.2 Point Defects in Crystals

The conductivity is very closely related to the existence of point defects in crystals. Defects may be generated in a solid by (1) thermodynamic equilibrium (Schottky, Frenkel), (2) chemical substitution, (3) oxidation or reduction, and (4) energetic radiation. Defects may be classified being either ionic defects (cation vacancies, cation interstitials, anion vacancies, and anion interstitials) or electronic defects (electrons and holes). In Table 2.4, Kroger-Vink [30] notation of the different types of defects are given.

The thermodynamic vacancy (Schottky) and interstitual (Frenkel) defects can be classified as inherent defects, since one or the other is always present in an ionic (crystal) solid at all temperatures above absolute zero [51]. Extrinsic defects are those defects present in an ionic solid as a result of doping with aliovalent ions and serve to preserve chemical stoichiometry.

Table 2.4 Ionic defect symbol

Symbol	Definition
M_M	Cation on regular lattice site
X_X	Anion on regular lattice site
V_M	Cation vacancy
V''_M	Effective charge on cation vacancy
M_i	Cation on interstitial site
$M_i^{\bullet\bullet}$	Effective charge on interstitial cation
X_i	Anion on interstitial site
X''_i	Effective charge on interstitial anion
V_X	Anion vacancy
$V_X^{\bullet\bullet}$	Effective charge on anion vacancy
$h^{\bullet}$	Positive hole
e'	Electron

The formation of these defects increases the configurational entropy of the solid, thereby decreasing the overall free energy. Relationships for Schottky defect formation may be given as:

$$M_M + X_X \rightarrow V''_M + V''_X \qquad (2-3)$$

Schottky defects are typically formed in close-packed structures such as MO oxides. The cation and anion vacancies are considered to form separately and migrate to the surface of the crystal, thereby increasing the volume and decreasing the density. Relationships for Frenkel defects may be written as:

$$M_M \rightarrow M_i^{\bullet\bullet} + V''_M \quad \text{or} \quad X_X \rightarrow X''_i + V_X^{\bullet\bullet} \qquad (2-4)$$

2.6.3 Defects in Metal oxides

Point defects that are formed in oxides as a result of equilibrium with the a gas phase ambient may occur by either oxygen deficiency (metal excess) or metal deficiency (oxygen excess) as follows [54]:

1) Oxygen deficiency (excess metal):

For such an oxide, the overall nonstoichiometric reaction can be written as

$$MO(s) \rightarrow MO_{1-x}(s) + \frac{x}{2} O_2(g) \qquad (2-5)$$

The oxygen vacancy is formed by the transfer of an oxygen atom on a normal lattice site to the gaseous shown as follows using Kroger-Vink notation:

$$O_O \rightarrow \frac{1}{2} O_2(g) + V_O^{\bullet\bullet} + 2e' \qquad (2-6)$$

Since the vacancy has two trapped electrons, it can act as a donar and become singly or doubly ionized. This leads to n-type conduction at high temperature in such fixed-valence oxides as Al_2O_3, Ga_2O_3, etc. The free electrons may also become associated with variable-valence cations and the following reactions can occur:

$$M_M + V_O \rightarrow V_O^{\bullet} + M'_M \qquad (2-7)$$

$$M'_M + V_O^{\bullet} \rightarrow V_O^{\bullet\bullet} + M''_M \qquad (2-8)$$

Equation (2 – 7) is the more likely reaction and leads to n-type hopping conduction in such oxides as TiO_2, Fe_2O_3, CeO_2, etc.

In the case of excess metal atoms, such atoms may be found in the interstices:

$$M_M + O_O \rightarrow M_i^{\bullet\bullet} + \frac{1}{2} O_2(g) + 2e'' \qquad (2-9)$$

The neutral M_i atom can subsequently be ionized:

$$M_i \rightarrow M_i^{\bullet} + e' \qquad (2-10)$$

$$M_i^{\bullet} \rightarrow M_i^{\bullet\bullet} + e' \qquad (2-11)$$

Again, the singly ionized state is the more likely and leads to n-type conduction in oxides such as ZnO.

2) Metal deficiency (excess oxygen):

In an oxide (MO) cation vacancies can be formed through the reaction of ambient oxygen with the oxide.

$$\frac{1}{2}O_2(g) \rightarrow V_M'' + O_O + 2h^{\bullet} \qquad (2-12)$$

The holes present in the vacancy may be excited and transferred to other parts of the crystal:

$$V_M \rightarrow V_M' + h^{\bullet} \qquad (2-13)$$

This condition leads to p-type conduction in such oxides as MnO, NiO, FeO, etc. As a valence defect, equation (2 – 13) can be written as

$$M_M + V_M \rightarrow V_M' + M_M^{\bullet} \qquad (2-14)$$

With excess oxygen, neutral interstitial oxygen atoms may be formed thus:

$$\frac{1}{2}O_2(g) \rightarrow O_i \qquad (2-15)$$

but this condition is not common in metal oxide lattices.

The relationship of oxygen partial pressure to conduction in metal deficient oxides can be illustrated as follows:

$$2M_M + \frac{1}{2}O_2(g) \rightarrow V_M'' + 2M_M^{\bullet} + O_O \qquad (2-16)$$

The equilibrium constant, K_T, for this reaction at temperature T is

$$K_T = \frac{[M_M^{\bullet}]^2[V_M^{''}][O_O]}{(P_{O_2})^{1/2}[M_M]^2} \qquad (2-17)$$

where [O_O] a nd [M_M] ~ 1 a nd $V_M^{''} = \frac{1}{2}[M_M^{\bullet}]$. Since σ, the conductivity, i s proportional to $[M_M^{\bullet}]$, the following relationship can be derived:

$$\sigma = KP_{O_2}^{1/6} \qquad (2-18)$$

Thus, i f t he P_{O_2} is i ncreased, t he c onductivity a lso i ncreases. I n oxyge n de ficient oxides such as Ga_2O_3 it can be shown, similarly, that the effect of increase in P_{O_2} is just the opposite, that is,

$$\sigma = KP_{O_2}^{-1/6} \qquad (2-19)$$

Depending on t he oxyg en pa rtial pr essure, therefore, n - or p -type c onduction may occur at very l ow a nd hi gh P_{O_2} , r espectively. F or P_{O_2} ranges w here t he oxyge n a nd metal v acancy co ncentrations are of si milar m agnitude, t he o xide is essen tially stoichiometric a nd i onic c onduction pr edominates [54]. A ll t hree t ypes of conductions a re exhibited by s uch oxi des ov er a w ide r ange of oxyge n pa rtial pressures.

3. Modeling and Simulation: Theoretical Study of Electrical Properties

3.1 INTRODUCTION

To understand the role of dopants in the electronic properties of gallium oxide, simulation and modelling of Ga_2O_3 was performed using a type of software called Materials Studio. In this section, Ga_2O_3coatings were simulated using this software and its electronic properties was studied theoretically [55].

3.2 OBJECTIVE OF THEORETICAL WORK

The objective of theoretical work with Materials Studio software is to study the effect of adding different dopants on the electrical properties of Ga_2O_3 structure. In particular, changing the lattice parameters and bandgap of Ga_2O_3 is studied after

doping with Sn^{4+}, Zn^{2+}, and W^{6+}. The justification for using these ions as dopants is that Sn^{4+}, W^{6+}, Zn^{2+} ions are close to Ga^{3+} in terms of ionic and covalent radius.

3.3 MATERIALS STUDIO SOFTWARE

Materials Studio is a flexible software environment for simulating and modeling the advanced materials. In this software, the calculation and analysis of functions are performed using CASTEP. CASTEP is a program that employs density functional theory (DFT) to simulate the crystal structure and properties of a wide range of materials classes based on total energy. CASTEP takes the number and type of atoms in a system and predicts properties including lattice constants, structural properties, band structures, density of states, etc. [55-57].

CASTEP can be used effectively to study properties of both point defects (vacancies, interstitials, and substitutional impurities) and extended defects (e.g. grain boundaries and dislocations) in semiconductors and other materials [56].

There are a number of steps involved in running a CASTEP calculation, which can be grouped as two items [55,58]: structure definition and calculation setup. Structure definition is a periodic 3D atomistic document containing the definition of the system of interest to be analysed. Once a suitable 3D structure document has been defined, the calculation setup is applied and then the type of calculation to be performed is selected and the associated parameters are set. Finally, the calculation that is to be run should be selected and the job initiated.

Final step which involved in a calculation is analysis of the results. When the calculation is complete, the files related to that job consist of results are analysed.

Some further processing of these files may be required to obtain observables such as electrical properties.

3.4 DOPING OF Ga_2O_3 WITH Sn, Zn, AND W

3.4.1 Details of Calculation

The program can be done in five stages as follow:

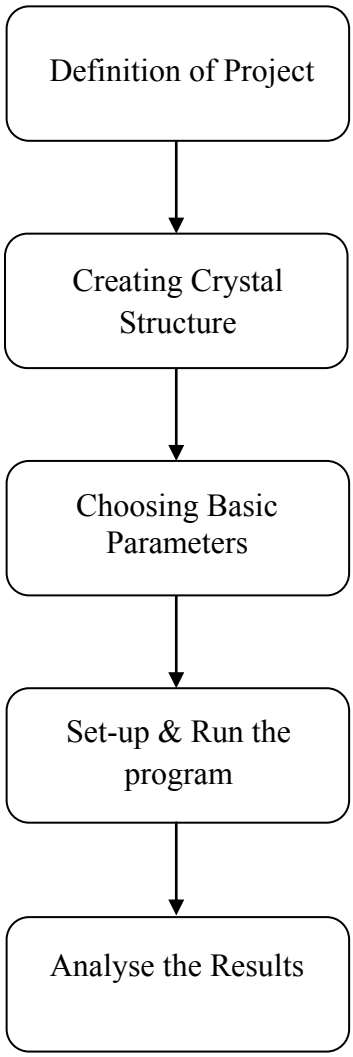

Fig. 3.1 Flow chart of processing steps for simulation of Ga_2O_3 structure [55]

First and second steps for modeling process shown in Fig. 3.1 are done based on crystal structure knowledge of the β-Ga_2O_3structure. The bandgap and lattice parameter changes on the intrinsic β-Ga_2O_3 structure are calculated based on density function theory after adding different percentages of Sn, Zn, and W dopant elements.

The conductivity of the intrinsic β-Ga_2O_3 is too poor to meet the requirements of applications. Selecting appropriate doping elements to improve the electrical conductivity is very important.

At normal conditions, Ga_2O_3 happens in the monoclinic (β) phase, although it may be transformed into four other high-pressure and temperature polymorphs.β-Ga_2O_3 belongs to space group C2/m with the two-fold rotation axis β [59]. In the unit cell,β-Ga_2O_3 has two different Ga sites, denoted as Ga(1) and Ga(2), and three different O sites, denoted as O(1), O(2), and O(3). To plot the β-Ga_2O_3 crystal structure using MS software shown in Fig. 3.2 (a), crystallography coordination (see Table 3.1) is required. Besides, unit cell and lattice parameters of this metal oxide should be considered. The unit cell can be characterized by four lattice parameters: *a*, *b*, *c*, and β. The Ga atoms are surrounded by O atoms in either tetrahedral Ga(1) or octahedral Ga(2) coordination.

Table 3.1 Crystallography coordination of β-Ga_2O_3[59]

Atomic site	Lattice positions		
	x	*y*	*z*
Ga(1)	0.1595	0.5000	0.3129
Ga(2)	0.0912	1.0000	0.7957
O(1)	0.1719	1.0000	0.5594
O(2)	0.3303	0.5000	0.8914
O(3)	0.9967	0.5000	0.2530

To dope the intrinsic Ga_2O_3, the Ga(2) atom is substituted by the dopant atom [58]. In this work, the crystal structure of β-Ga_2O_3 was doped with Sn, W, and Zn shown in Fig. 3.2 (b, c, and d).

All the calculations were completed by CASTEP [59, 60]software package in Materials Studio Version 4.4 software. In this software, choosing basic parameters for set up the program is another step. It should be chosen based on the quality type which is course, medium, and fine. The differences between qualities affect the rate and time of program (e.g. fine quality in this program is the most time-consuming work). In this work, fine quality was considered and based on that, these basic parameters were set up and run. After completing the program which took a time of 1 to 3 days for each program, the results are analyzed and the bandgap and changes in lattice parameters are obtained.

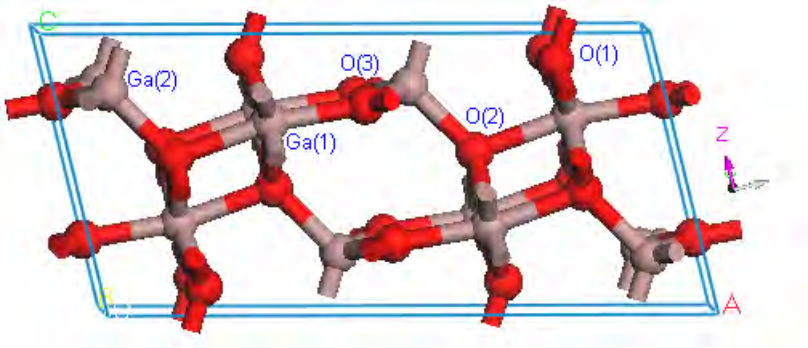

(a)

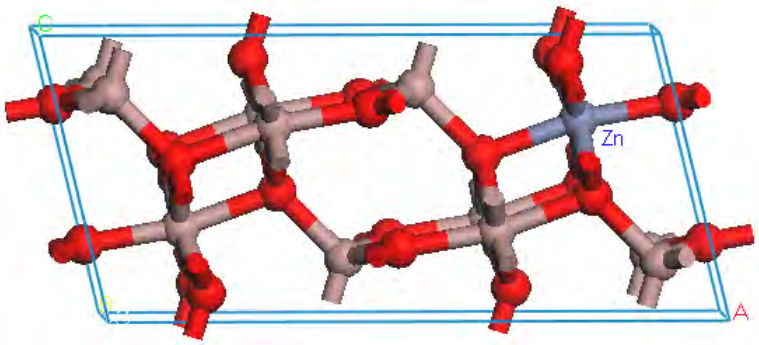

(b)

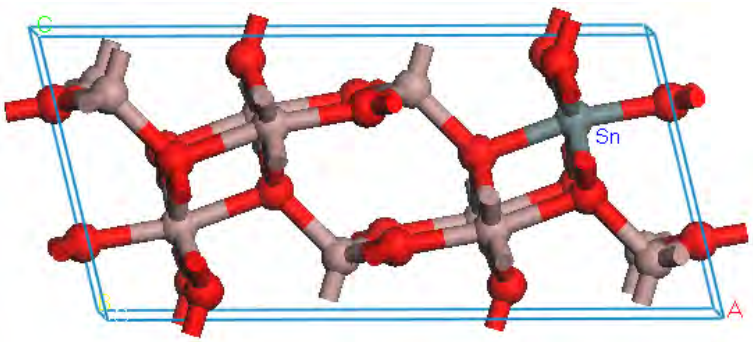

(c)

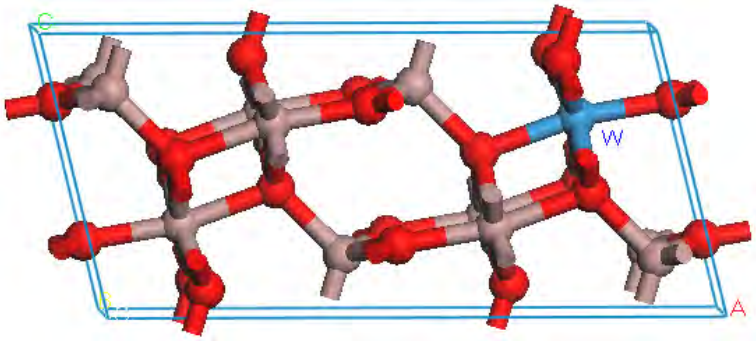

(d)

Fig. 3.2 Crystal structure of (a) intrinsic Ga_2O_3, (b) Zn-doped Ga_2O_3, (c) Sn-doped Ga_2O_3, (d) W-doped Ga_2O_3

3.5 Simulation Results and Discussion

3.5.1 Geometrical structures

The geometry optimization is shown as a diagram in Fig. 3.3. The equilibrium structure was obtained after the cell geometry and volume were fully relaxed by minimizing the total energy and forces [52, 58].

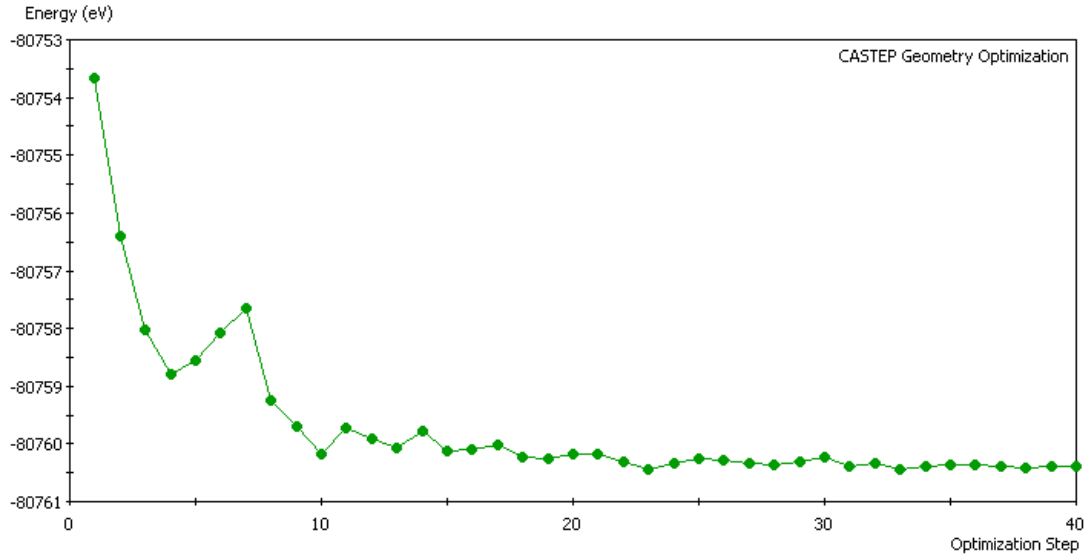

Fig. 3.3 Energy optimization of Ga_2O_3

Before adding different percentages of dopant to Ga_2O_3 structure, energy optimization is carried out (Fig. 3.3). The reason is to make sure that running the program is done accurately to obtain convergence. This diagram (Fig. 3.3) shows that there is a convergence and, thus the results are acceptable.

The calculated equilibrium lattice constants of the intrinsic and doped β-Ga_2O_3 are shown in Table 3.2. The results for intrinsic Ga_2O_3 are similar to values reported in literature [19] indicating that choosing basic parameters used in the model are completely matched with crystal structure and crystal project definition, and that the simulation has been done correctly. For both, the lattice angles have not changed from literature [19] and little change exists in the lattice length.

The lattice parameters, crystal volume, and bandgap change of β-Ga_2O_3 doped with the various dopants (3.125-12.5%) are tabulated in Table 3.2. Note that all dopant percentages are wt%.

Table 3.2 Intrinsic and different concentration of dopants in Ga_2O_3

Material	a (nm)	b (nm)	c (nm)	α	β	γ	V (A^3)	E_g (eV)
Intrinsic Ga_2O_3	125.3	31.0	59.0	90	103.8	90	217.6	2.315
Reference[19]	122.3	30.4	58.0	90	103.8	90	217.7	2.190
3.125% Sn	132.1	33.0	60.2	90	103.6	90	236.9	1.600
6.250% Sn	132.5	33.1	60.2	90	103.4	90	240.1	1.097
9.375% Sn	133.3	33.3	60.4	90	103.3	90	244.2	0.665
12.50% Sn	134.0	33.5	60.7	90	103.5	90	247.2	0.215
3.125% Zn	132.9	33.2	60.1	90	103.6	90	237.5	2.260
6.250% Zn	132.3	33.0	59.8	90	103.4	90	236.1	1.415
9.375% Zn	133.2	33.3	60.0	90	103.4	90	238.4	0.945
12.50% Zn	134.0	33.4	60.0	90	103.0	90	238.8	0.445
3.125% W	132.0	33.0	60.3	90	103.6	90	237.7	2.100
6.250% W	134.9	33.7	60.3	90	103.4	90	246.0	1.600
9.375% W	132.1	33.3	60.4	90	104.3	90	244.2	1.450
12.5% W	No Convergence							

Fig. 3.4 and Fig. 3.5 present lattice parameter (a) and bandgap values as a function of changes of dopant percentage to compare the parameters' change in crystal structure of Ga_2O_3. No significant changes were observed for lattice parameters b and c.

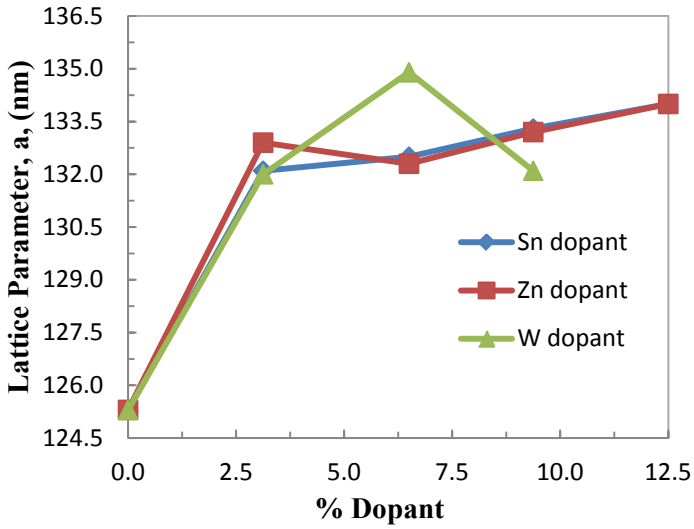

Fig. 3.4 Changes in lattice parameter, a, vs. different percentage of dopants (wt%)

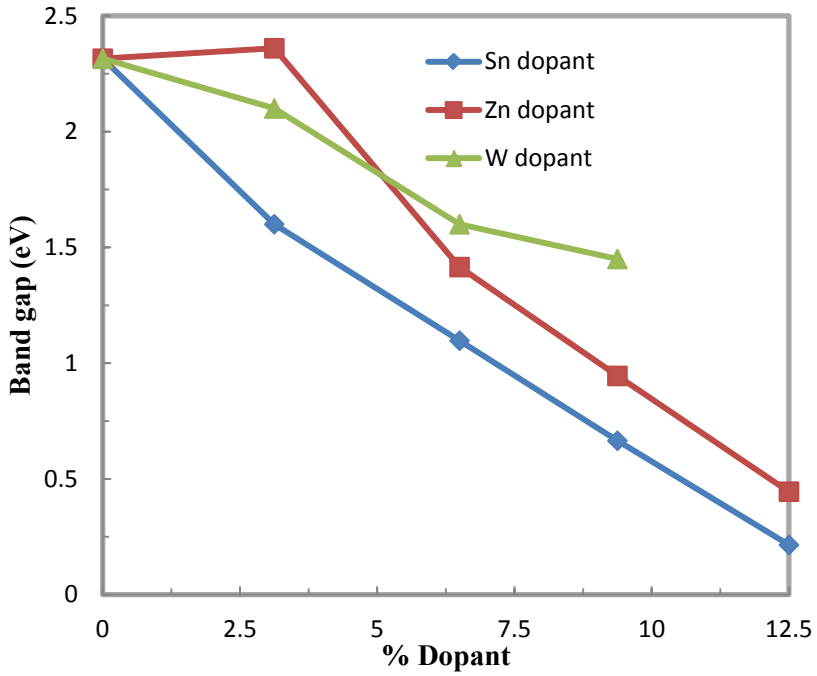

Fig. 3.5 Changes in bandgap vs. different percentage of dopants (wt%)

Fig. 3.4 shows that the lattice parameter, a, has totally increased after doping. Increasing to 3.175% of each dopants leads to an increase of 7 nm in this lattice parameter. For percentage of dopants more than 3.175 %, changing in lattice

parameter of Ga_2O_3 crystal structure doped with Zn and Sn are almost similar to each other. However, for W the differences in lattice parameters are more pronounced. It might be due to the difference in ionic and covalent radii of Ga^{3+} ion and W^{6+} (see Table 3.3). Ionic and covalent radii of dopant ions should be comparable with Ga^{3+} to be replaced with this main atom. The ionic (and covalent) size of Sn^{4+}, Zn^{2+} and Ga^{3+}(shown in Table 3.3) are very close to each other, that is 0.69 (1.41), 0.74 (1.22), and 0.62 (1.26) nm, respectively (from Pauling's ionic radii data). For W^{6+}, these values are 0.78 (1.62) nm which present a more deviation from $\frac{R_{Ga^{3+}}}{R_{dopant}}=1$ than Sn^{4+} and Zn^{2+}. On the other hand, contribution of significantly different valence of W^{6+} from Ga^{3+} on the lattice parameter could not be considered negligible. As a result, no convergence occurred when the weight percentage of W in Ga_2O_3 structure increased to 12.5%.

Fig. 3.5 shows the bandgap change in Ga_2O_3 crystal structure after doping with different percentages of Sn, Zn, and W elements. From this diagram, it can be seen that Sn ions present more reduction in the bandgap compared to the other investigated Zn and W ions. The bandgap in intrinsic Ga_2O_3 is approximately 2.315 eV. It was reduced to 1.6 after adding 3.125 % Sn ions. This ion causes more decrease in bandgap i.e. from 1.6 to 0.215 eV when the amount of Sn concentration goes from 3.125% to 12.5%. This amount is much more compared to Zn and W ions. The calculated bandgap for intrinsic Ga_2O_3 is 2.315eV. Theoretical bandgap and experimental bandgap values have a large disparity. As we know, the bandgap of intrinsic Ga_2O_3 is almost 4.9 eV. This is because DFT theory is based on the ground state theoretically, resulting in the exchange–correlation potential between the excited electronic that have been underestimated[57].

Table 3.3 Ionic and covalent radius, and radii ratio of different elements [61]

	Ga^{3+}	Sn^{4+}	Zn^{2+}	W^{6+}
Ionic Radius (Å)	0.62	0.83	0.74	0.78
Covalent Radius (Å)	1.23	1.40	1.22	1.62
$\frac{R_{Ga^{3+}}}{R_{dopant}}$	1.000	0.894	1.030	0.770

On the other hand, based on point defect chemistry [Kroger-Vink], explained in section 2.5.2, Zn^{2+}, Sn^{4+}, and W^{6+} can go into the lattice as substitutional dopants. Sn^{4+} and W^{6+} may act as donors, while Zn^{2+} may act as an acceptor. The incorporation of Sn, Zn, and W in Ga_2O_3 can be described by the following reactions:

$$ZnO \rightarrow Zn''_{Ga} + V_O^{\bullet\bullet} + O_O \qquad (4-1)$$

$$W_2O_6 \rightarrow 2\,W_{Ga}^{\bullet\bullet} + V''_{Ga} + 6\,O_O \qquad (4-2)$$

$$SnO_2 \rightarrow Sn_{Ga}^{\bullet\bullet} + V''_{Ga} + 2\,O_O \qquad (4-3)$$

These dopants can dramatically affect the electrical properties of Ga_2O_3. The addition of Zn to Ga_2O_3 increases the conductivity.

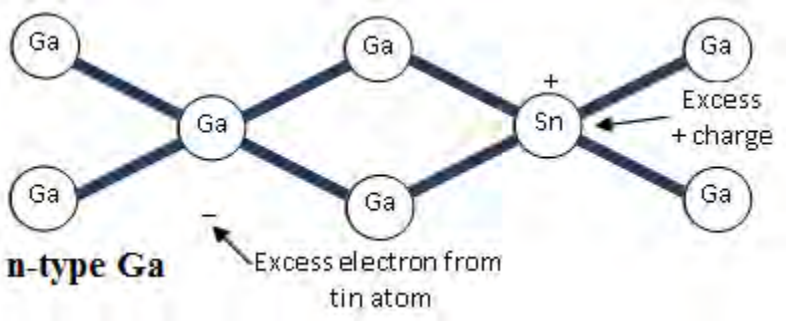

Fig. 3.6 Charges associated with a Sn dopant in Ga

Sn has four valence electrons, but Ga has only three valence electrons. Therefore, three electrons of the Sn form similar bonds with Ga, and the fourth electron is available for conduction, indicating Sn is a donor dopant in Ga_2O_3 (see Fig. 3.6).

Charges associated with a W ion in Ga_2O_3 are shown schematically in Fig. 3.7. W has six valence electrons while Ga has only three valence electrons. Therefore, three electrons of the W form three localised bonds with oxygen, while the three electrons in excess are available for conduction, thus suggesting that W atoms act as donor dopants in Ga_2O_3 (Fig. 3.8).

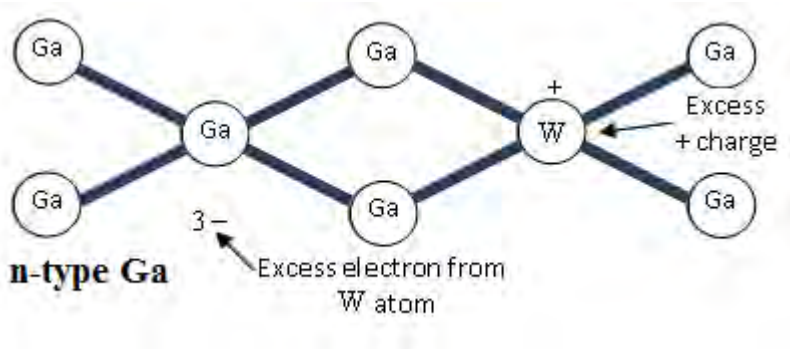

Fig. 3.7 Charges associated with a W dopant atom in Ga_2O_3

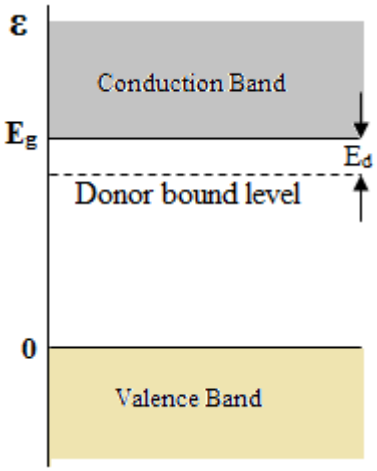

Fig. 3.8 Donor bond level in electrical conduction bond

The addition of Sn or W to Ga_2O_3 is different from Zn. Zn has only two valence electrons; it can complete its bonds only by taking an electron from a Ga-Ga bond, leaving behind a hole in the Ga valence band. The positive hole is then available for conduction. Therefore, Zn atom is an acceptor because when ionized it accepts an

electron from the valence band. The schematic for this electron exchange is shown in Fig. 3.9 and Fig. 3.10.

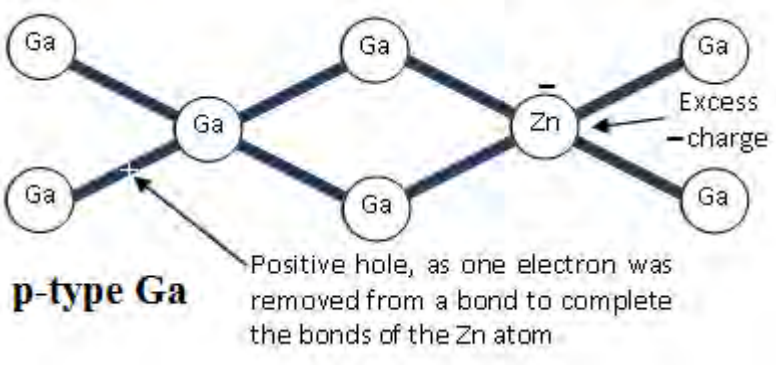

Fig. 3.9 Charges associated with a Zn atom in Ga

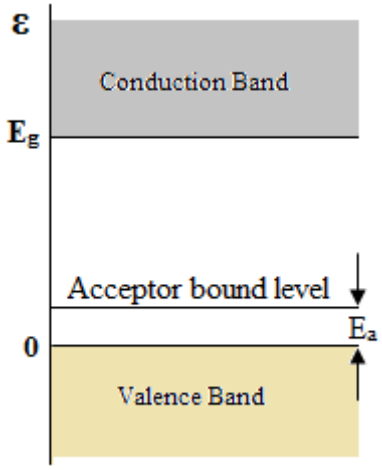

Fig. 3.10 Acceptor bond level in electrical conduction bond

In summary, the effect of dopants on the electronic property of β-Ga_2O_3 was analyzed. The introduction of the Sn and Zn caused the impurity energy level at the bottom of the conduction band. Therefore, the conductivity of the Zn-doped and Sn-doped β-Ga_2O_3 is basically improved compared to the intrinsic β-Ga_2O_3.

4. Experimental Procedure

4.1 INTRODUCTION

As examined previously, Ga_2O_3 coating deposited on ceramic substrates such as quartz via sol-gel routes has been reported as promising candidate for many applications. In general, however, cracking of coatings at the drying stage of sol-gel processing is one of the main problems encountered in forming stable, thick coatings and is caused usually by high shrinkage during drying and/or firing. To solve this problem, understanding the colloidal behaviour of gallium-oxide particles in solution and the formation of stable sol is important. Ga_2O_3 sol-gel processing involving controlled hydrolysis and condensation, peptisation, gellation, drying and consolidation by a Ga-propoxide route is studied in this work.

4.2 OBJECTIVE OF EXPERIMENTAL WORK

The objective of the experimental work presented in this chapter was to develop Ga_2O_3 sol-gel coating layers on suitable ceramic substrates such as quartz with minimal or no cracking on coating, and to investigate the structure and morphology of coating. The work involved two main areas of research. Firstly, the preparation of coating solutions and their deposition drying and gelation were investigated. Secondly, the drying and heat-treatment of coatings and the effect of heat-treatment parameters on the cracking behaviour of coating and microstructural during drying and firing were studied. Also, incorporation of suitable ions, as solid solution dopants for Ga^{3+} in Ga_2O_3, in the sol-gel process were investigated.

4.3 EXPERIMENTAL PROCEDURE

The general experimental procedure for sol-gel preparation of gallium oxide coatings on substrates (glass and quartz) is summarized in Fig. 4.1. Two procedures were used: Type-II sol based on an aqueous route developed for Al_2O_3 by Yoldas [38], and Type-I sol based on MOE. As explained later, sol-gel coatings prepared from the Type-I route did not gelate (hence could not gel coherent coatings) and this necessitated the developments of the non-aqueous route.

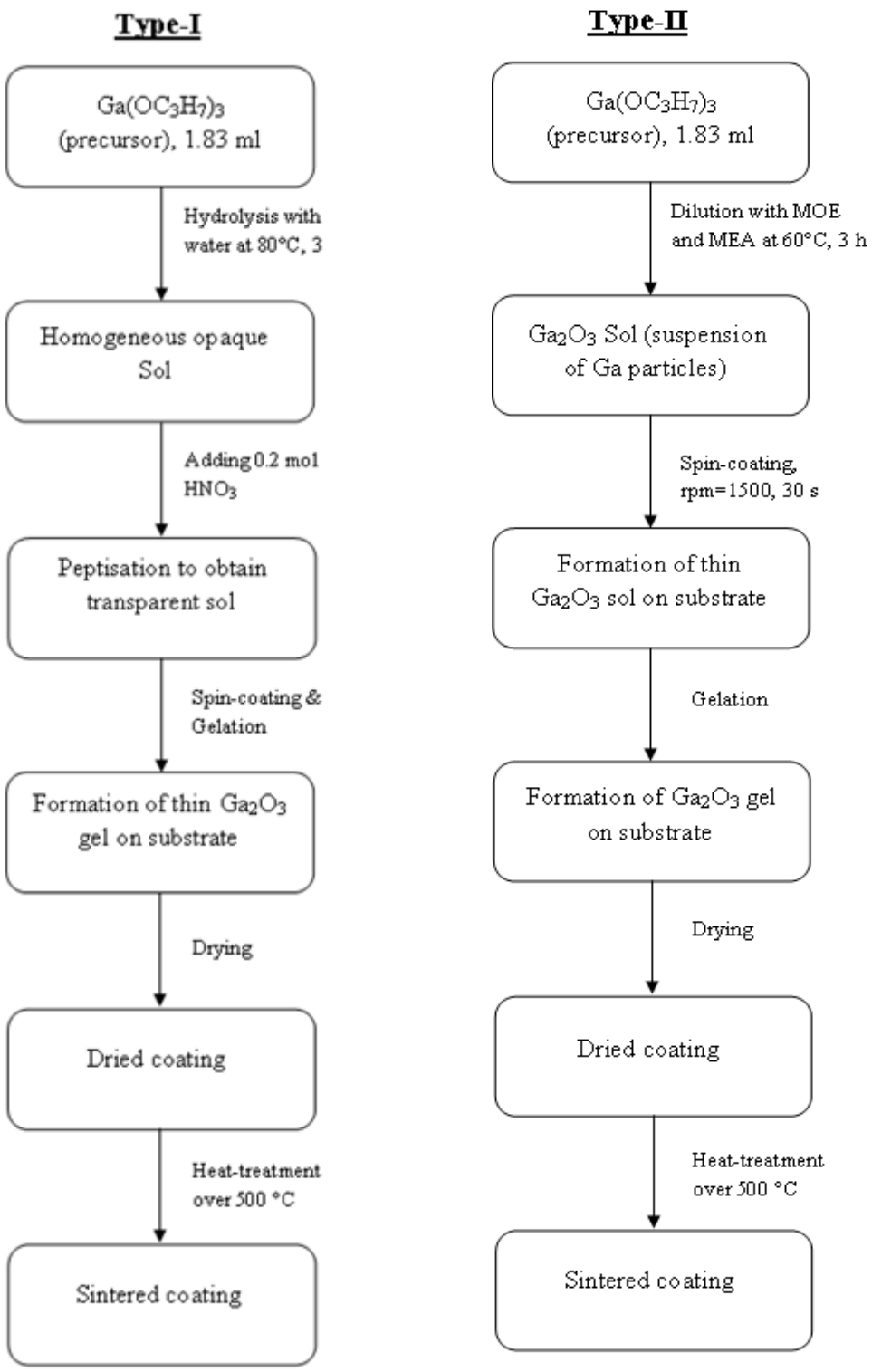

Fig. 4.1 Overall flow chart of experimental procedure [38, 47]

4.3.1 Preparation of Coating Solution

Aqueous Route (sol Type-I)

As indicated in Fig. 4.1, a gallium mono-hydroxide (GaOOH) sol for producing Ga_2O_3 coating on substrate was prepared by a method similar to the method reported by Yoldas [38]. A total of 1.83 ml (0.01 mol) gallium-isopropoxide, < $Ga(OC_3H_7)_3$, 99.9 wt% purity, Multivalent Lab. Co. UK >, was slowly dripped into 20 ml (~1 mol) de-ionised stirred water held at temperature of 75°C. This was done in a sealed flask immersed in a controlled-temperature silicon-oil bath and fitted with a thermometer and condenser (Fig. 4.2). The solution was stirred continuously during the addition of gallium-propoxide and then for a further for 30 minute to obtain a homogenous opaque solution. Then, 0.05 mL (0.2 mol) nitric acid (HNO_3, 70%, Sigma-aldrich) was added to peptize the hydrolysed solution, followed by stirring at 85-90°C for 24 hours. After peptisation, the sol was removed from the flask and stored in a sealed glass bottle at room temperature. The pH of this solution was measured using a pH-meter calibrated against standard buffered pH solutions.

Non-Aqueous Route (sol Type-II)

The above aqueous technique based on Yoldas's method [38] did not provide a transparent uniform colloidal sol. Therefore, a non-aqueous method as explained in this section was utilised. In this technique, a gallium-alkoxide such as gallium-isopropoxide was dissolved in a non-aqueous solvent and stabilizer over the temperature range of 60-80˚C. 2-Methoxyethanol (MOE) and monoethanolamine (MEA) were used as the solvent and stabilizer, respectively. GaP was first dissolved in a mixture of MOE and MEA at 60°C using similar reaction set-up to the described

above (Fig. 4.2) . The molar r atio of M EA t o GaP was maintained a t 1.0 a nd t he concentration of GaP was 0.2 and 0.4 mol/L. After the solution was stirred for 1 h, a homogeneous and transparent solution was obtained. To provide a 50 ml of this sol, 3.65 ml of GaP w as a dded t o s olution of 45.0 a nd 1.5 ml of M OE a nd M EA, respectively. E xcess waste $Ga(OC_3H_7)_3$ was diluted i n ethanol a nd then a dded t o excess w ater an d d isposed b y co ntract w aste disposal. Unwanted s ol-gel s olution was disposed by contract waste disposal.

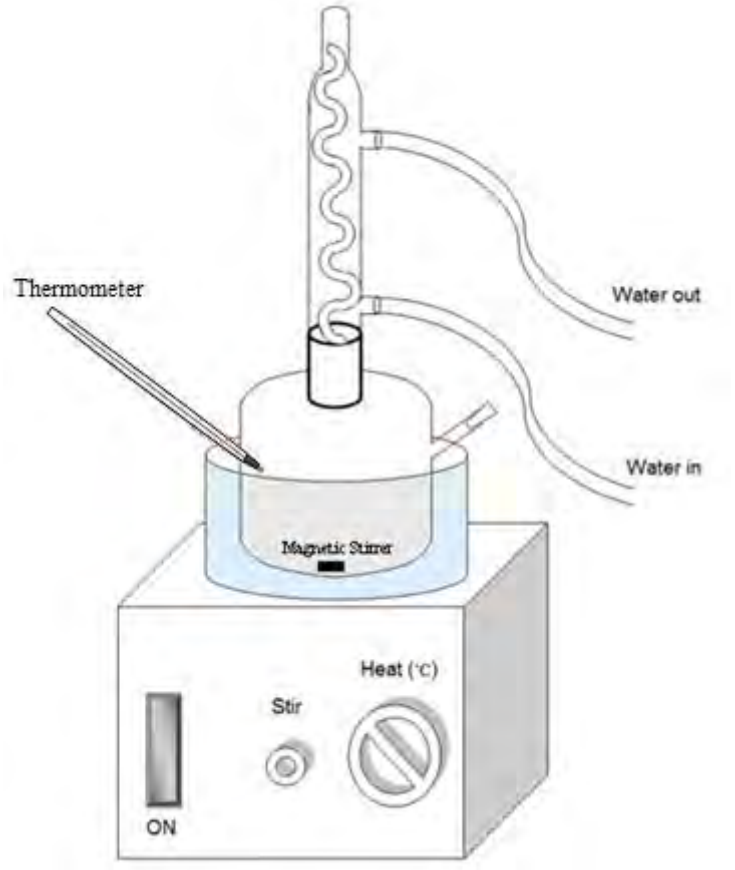

Fig. 4.2 Schematic diagram of reaction equipment for Ga_2O_3 sol

GaP i s a corrosive material a nd i s da ngerous to s kin a nd e yes, as well b eing flammable a nd s o pr ecautions a re essential f or t he s torage a nd ha ndling of t his material. Containers which are opened must be carefully resealed to prevent leakage.

Also a bottle containing only a small quantity (<25g) of the chemical is kept and this bottle is sealed inside a larger plastic container. For the solution preparation, the chemical was handled under an inert atmosphere of argon in a glove box or glove bag; with atmosphere being exhausted within a fume cupboard.

4.3.2 Preparation of doped Ga_2O_3 Solution

Sol-Gel routes for preparing doped-Ga_2O_3 have not been reported in the literature. The non-aqueous route described above (Type-II sol) was found to be successful for the pure Ga_2O_3 coatings and so was modified to incorporate dopant cations. The procedure is summarized in Fig. 4.3 [62, 63].

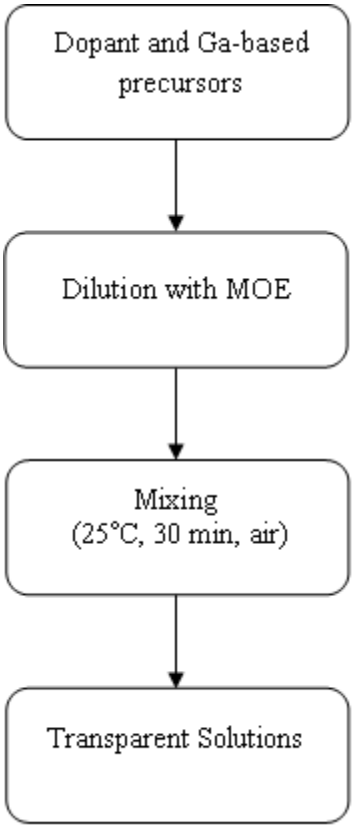

Fig. 4.3 Flow chart of sol-gel processing for preparation of doped Ga_2O_3 solution

In these experiments, the precursors were first weighed out and then compound of dopants (nitrate or chloride) which were in the powder form were dissolved in MOE. In some work [10, 41, 63] isopropanol is used as solvent, but MOE was used here because it is a better solvent for gallium propoxide (GaP) than isopropanol. Gallium isopropoxide was incorporated into the mixture. The obtained solutions were stirred for 30 minutes in an open receptacle and kept at room temperature in air in order to yield a clear and homogeneous solution.

Since Gallium and aluminium are in a same group in the periodic table of the elements, and the chemical and physical behaviors of their oxides are generally comparable with each other, a comparison between these two metal oxides were performed in terms of resultant solutions with varied dopants. To compare doped Ga_2O_3 and Al_2O_3, with the same method above mentioned, aluminium butoxide was used in the mixture instead of gallium isopropoxide.

To dope Ga_2O_3 sol with different concentration of dopants, the dopants which would be compatible with Ga_2O_3 had to first be determined. To choose dopants for a solution, besides the electronic preparation of the final ceramic structure, the ionic and covalent radius should be considered. In particular, an ionic / covalent radius of the dopant cation should be close to gallium, thus the dopant ions could go into the lattice as substitutional dopants. Table 4.1 lists Pauling's ionic and covalent radii data of some potential ions as dopants for Ga^{3+}.

Table 4.1 Ionic and covalent radius of different ions [64]

	Ga^{3+}	Sn^{4+}	Zn^{2+}	W^{6+}	Mn^{2+}	Cu^{2+}	Al^{3+}
Ionic Radius (Å)	0.62	0.83	0.74	0.78	0.72	0.73	0.53
Covalent Radius (Å)	1.23	1.4	1.22	1.62	1.17	1.17	1.18

According to data in table 4.1, the best ions as dopants for Ga^{3+} might be Zn^{2+}, Mn^{2+}, and Cu^{2+}. Thus, Ga_2O_3 solution was doped with these dopants. The reaction of these ions with Ga^{3+} resulted in a homogenous and transparent solution. The first issue that was faced was the suitability of the technique to make a solution of dopant and Ga^{3+}. Although, in simulation of Ga_2O_3 using MS software, explained in section 3, Sn^{4+}, W^{6+}, Zn^{2+} ions have been chosen as dopants which are near Ga^{3+} in terms of ionic and covalent radius, Zn^{2+}, Mn^{2+}, Cu^{2+} were selected for this aim. It was due to the limitation of time and dopant compound as well as the precipitation issues of particles during the reaction. To compare the consistency between simulation results and experiment result, Zn-doped Ga_2O_3 and pure Ga_2O_3 coating were selected for the measurement. Since different percentages of dopants were employed in the simulation, two varied percentages of Zn-doped Ga_2O_3 (i.e. 3% and 6% of Zn) was produced for the measurement of bandgap on these coatings.

4.3.3 Deposition of Coatings

The substrates used in this work were quartz (α-quartz; 15 mm diameter x 1 mm thick disks; Highborn Co. Taiwan) and glass (soda-lime-silicate glass; 20 mm x 20 mm x 1 mm thick; Shanghai Machinery Import and Export Company, China). Prior to sol-gel deposition, the substrates were degreased with solvent (acetone) in an

ultrasonic bath and dried with compressed air. Then, sols were deposited onto substrate discs using a spin coater (in-house unit, School of Materials Science and Engineering, UNSW). The substrate was aligned with the centre of the spin coater. A syringe was used to deposit the prepared coating solution onto the substrate which was rotating at minimal speed (~5 rpm). The speed of the spin coater then was increased to 1500 rpm and maintained at this speed for 30 seconds (Fig. 4.4) to create a thin uniform coating on the substrate. To build up varied coating thicknesses, spin coating was performed in several times. As explained later and based on SEM images, each spin coating layer was almost 50 nm.

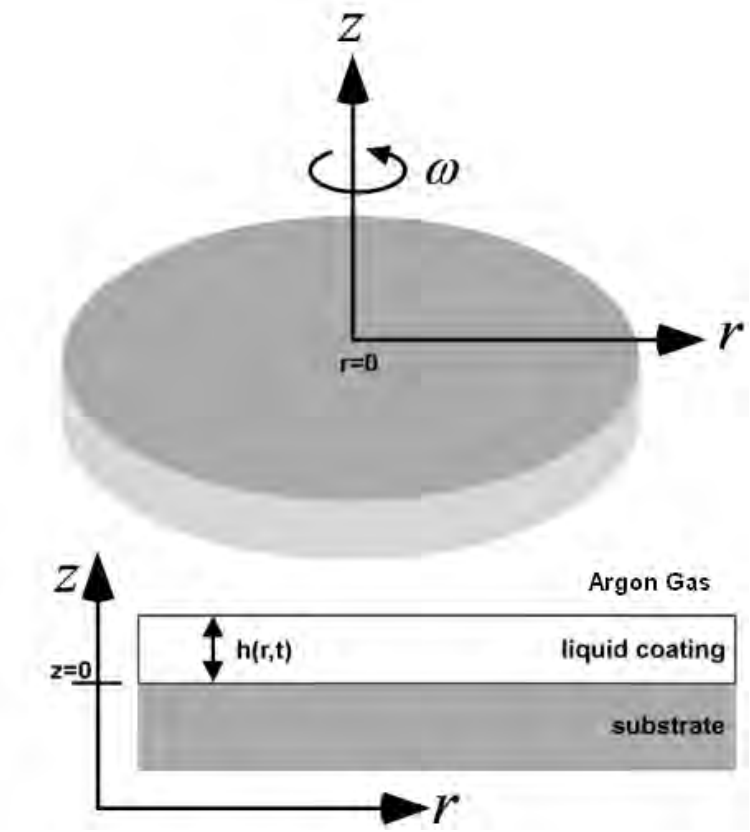

Fig. 4.4 Schematic diagram of spin coating method

4.3.4 Drying and Heat-treatment

After spin coating, coated substrates were dried slowly in air (25˚C) for one hour to decrease the risk of cracking on coating due to quick evaporation. The dried substrates then heated at 90˚C in an electrical oven for 10 min to evaporate the solvent, and then at 300°C for 20 min to eliminate the organic component in the coating. The dried coatings were then heated at 2 and 5˚C/min to a soak temperature over 300 ˚C in an electrical muffle furnace (Industrial Heating Engineers, Kiln Factory, NSW, AU). The thickness of the coating was estimated (using SEM) to be around 50-400 nm.

4.4 CHARACTERIZATION OF PREPARED SOLS

4.4.1 Viscosity

The viscosity measurements were performed on Type-I and Type-II sols using a Programmable Rheometer, Brookfield model DV-III. The main result of this characterization indicated the viscosity-time-temperature interactions in the sols and, in particular, the onset of gelation.

4.4.2 FTIR (Fourier Transform Infrared Spectroscopy)

Structural evolution of sol–gel gallium oxide in solution was investigated on scales of several lengths using infrared spectroscopy. FTIR of sol type I and II were performed using a spectrometer (Perkin-Elmer 2000).

4.5 CHARACTERIZATON OF COATED SAMPLES

4.5.1 Coating Morphology

The surfaces of samples were inspected after each stage of coating and heat treatment using reflected-light optical microscopy (Epiphot 600, Nikon, Japan) to evaluate the coating quality and, in particular, the extent of cracking.

4.5.2 Phase Composition

The phase composition of fired coatings on substrate discs were analysed using thin film X-ray diffraction (XRD; X'Pert PRO MRD, Philips diffractometer Model 1820 with CuK_{α} 0.15 nm at 45 KV/40mA). The incidence angle of the X-ray beam was either 0.8˚ or 2.0˚ and the scan range was 20˚-80˚ using a step size of 0.02˚ at step duration of 1.5 seconds (0.8˚/min).

The resultant data were analysed using propriety software (Traces v3.0, EMU, UNSW). The crystalline phases were identified according to phases contained in the ICDD Powder Diffraction File.

4.5.3 Microstructure and Composition

The microstructures of the fired coatings were examined using scanning electron microscopy (SEM; Model S230, Hitachi, Japan) was used to examine the coatings at high magnification (>1000X). Coated substrates after heating at different temperatures (over 300˚C) were sputter-coated with gold for SEM analysis. Energy-dispersive spectrometry (EDS) microanalysis (Oxford Instruments Link ISIS, EMU, UNSW) using SEM with an acceleration voltage of 10-15 kV was used to determine

the chemical composition of the fired coatings. At least five analyses at different spots were performed for each sample to obtain an average composition value.

4.5.4 Bandgap Measurement

The optical bandgap energy of sol–gel gallium oxide and Zn-doped Ga_2O_3 coatings with different percentages (3% and 6%) was measured using an ultraviolet-visible-near infrared spectrometer (Perkin Elmer UV/VIS/NIR Lambda 950). The transmittance spectrum of the coatings was recorded from 200 to 800 nm with the wavelength corresponding to the optical bandgap being determined by linear extrapolation of the lower-wavelength portion of the plot to zero percent transmittance. The optical bandgap was then calculated from this wavelength using Planck's equation. Given that for almost all inorganic semiconductors, including Ga_2O_3, there is very little interaction between electrons and holes, the optical and electronic bandgap are virtually identical and thus the optical bandgap values measured in this work could be used reliably as values of the electronic bandgap.

5. Results and Interpretation

5.1 QUALITY EVALUATION OF SOLS

5.1.1 Viscometry

The result of viscometry and required time of sol for converting to gel are shown in Fig. 5.1. From these results, it can be found out that in less amount of time the Type-II sol could convert to gel. Type-I coated substrates were not able to form coating after drying and sintering. Based on this measurement, there is no gelation in Type-I sol after 160 minutes while Type-II sol tended to convert to gel after about 60 minutes. This is in agreement with optical microscopy images and the SEM images shown in Section 5.2.

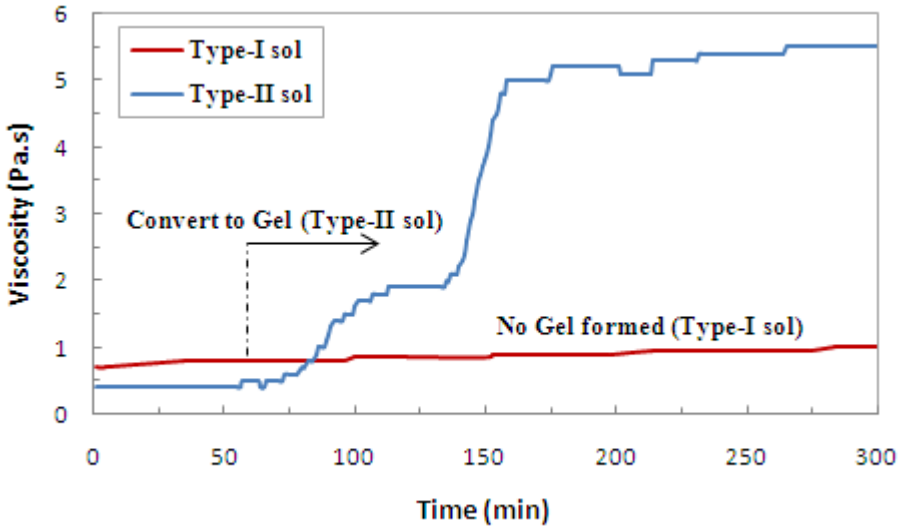

Fig. 5.1 Rheology behaviour of Type-I and Type-II sols

5.1.2 FTIR Results

All so lutions w ere ch aracterized by F T-IR s pectroscopy. Fig. 5.2 shows FT-IR spectra of selected samples which are Type-I and Type-II sols. The spectra of these sols show similar spectral features.

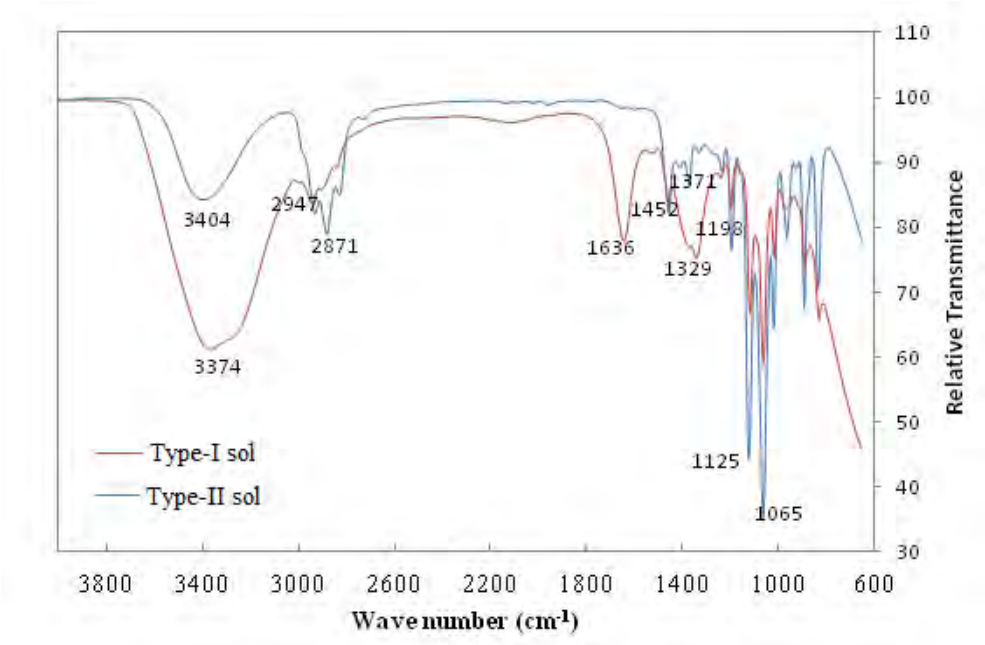

Fig. 5.2 Fourier Transform Infrared of Type-I and Type-II sols

A very strong and broad band at 3404 and 3374cm^{-1} can be assigned to –OH stretching vibrations of H_2O molecules. The stretching band of structural –OH groups is not separated due to strong overlap by the band at 3404cm^{-1}. The IR band at 1452 cm^{-1} is due to –OH bending vibrations of H_2O molecules. The presence of the bands at 1371 and 1198 cm^{-1} can be assigned to –COO vibrations which have been previously reported[27, 65]. The IR bands at 1125 and 1065 cm^{-1} for sol type I and II can be assigned to δ (OH) deformation vibrations. Therefore they can be assigned to Ga–OH vibrations. Although viscosity results show that these sols are completely different in terms of quality and converting to gel, structural evolution of these sols are not so different from each other. FTIR of sols indicates that band characteristic exist in sols are almost similar to each other in high wave numbers.

5.2 MICROSTRUCTURE OF COATED SAMPLES

5.2.1 Examination by Optical Microscopy

Figures 5.3 to 5.7 show the reflected-light optical microscope images of sol-gel Ga_2O_3 coatings produced from the two types of sols (I and II) with varied experimental parameters on glass substrates. Samples in Fig. 5.3 shows coating from Type-I sol and Fig. 5.4 to 5.7 show coatings from Type-II sol.

Fig. 5.3 shows the microstructure of sample heated for 2 h at different temperatures (300, 400, and 500°C) with heating rate of 2˚C/min and predicted thickness of 400 nm. Fig. 5.4 shows the microstructures of samples heated for 2 h at 300˚C with different heating rates (2˚C/min and 5˚C/min) and different thicknesses (200 nm and 400 nm). This experiment was repeated for two other soak temperatures of 400˚C

and 500˚C with the same conditions of heating rate and sample thicknesses, which the resultant microstructures shown in Fig. 5.5 and 5.6, respectively.

For samples which were provided from sol Type-I, there was a problem with forming the gel. Due to this problem, no coatings formed in substrate after heating in various temperatures (Fig. 5.3).

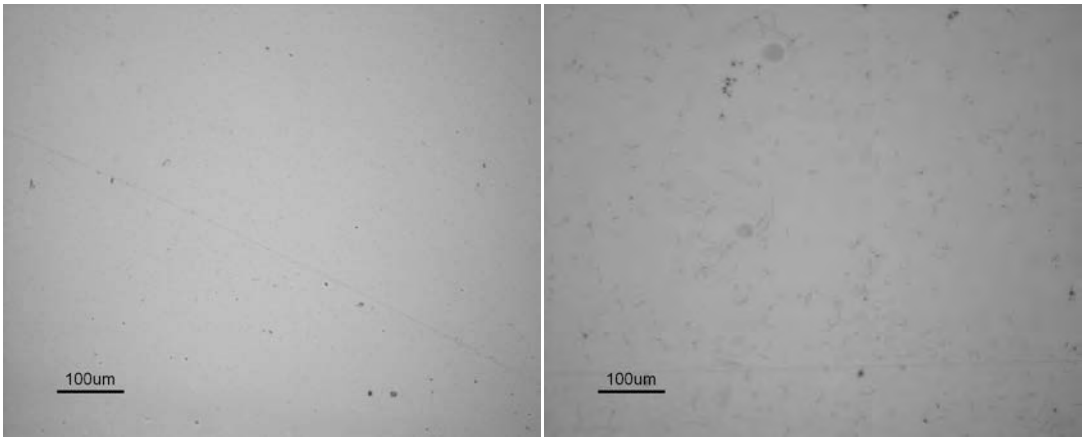

(a) (b)

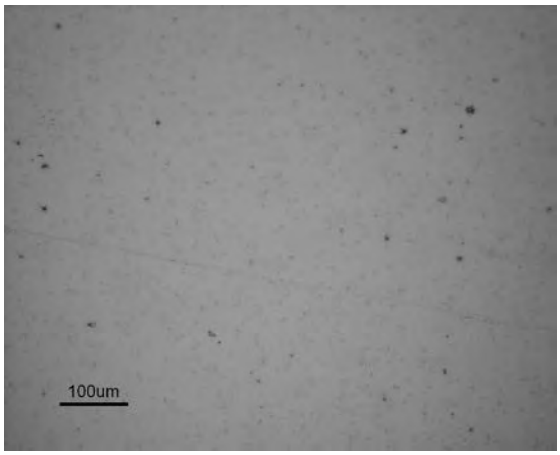

(c)

Fig. 5.3 Sol-gel Ga_2O_3 thin film, Type-I sol, heating rate of 2˚C/min, 8 spin-coating layers (predicted thickness of coating is 400 nm) (a) heating at 300˚C for 2 h, (b) heating at 400˚C for 2 h, (c) heating at 500˚C for 2 h

Coatings produced from the Type II (non aqueous sol) are now considered. As can be seen in Fig.5.4, for a soak time of 300°C, increasing heating rate and thickness of coatings tended to increase the extent of cracking in the coatings.

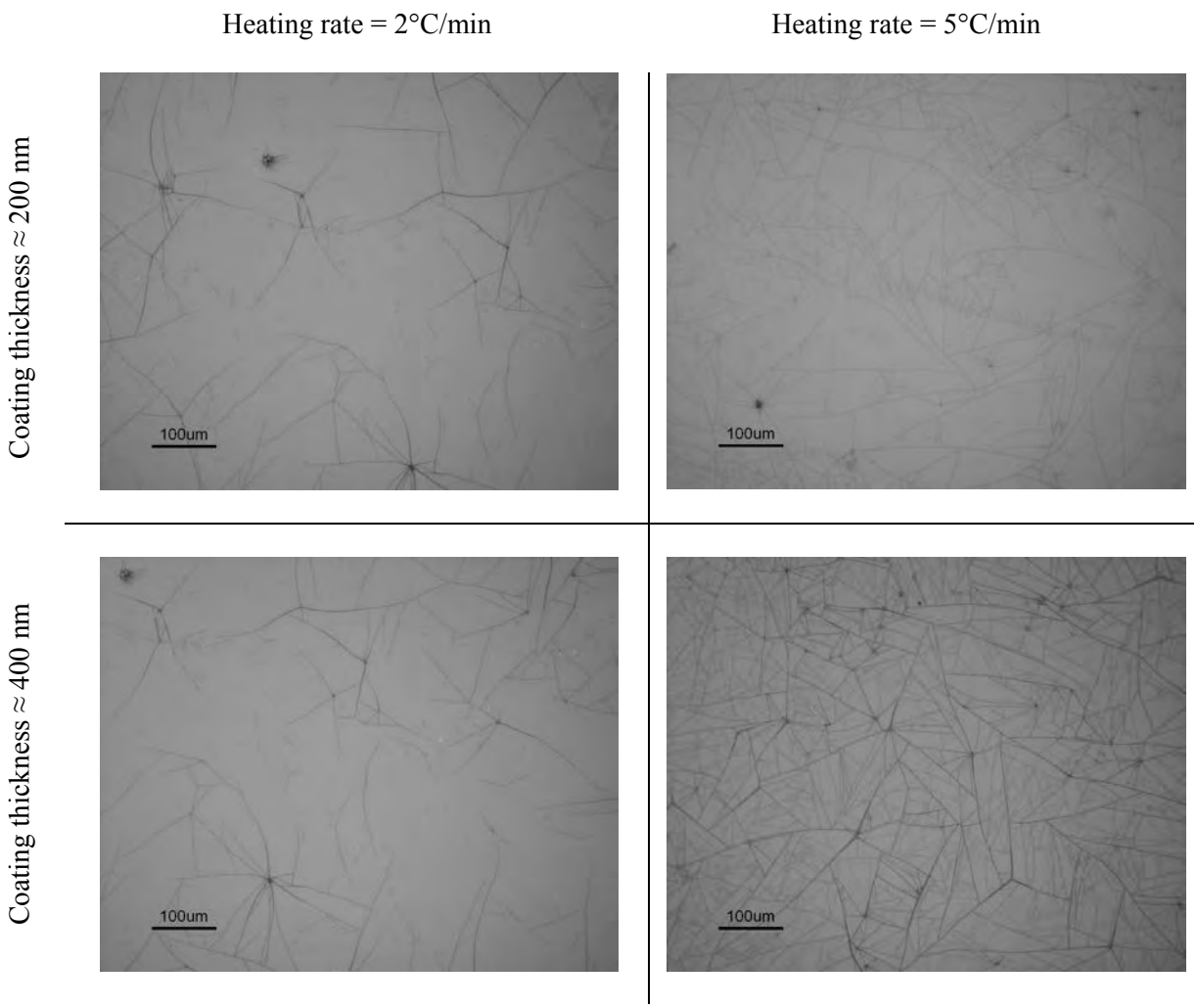

Fig. 5.4 Sol-gel Ga_2O_3 thin film, Type-II sol, on glass substrate, produced by heating at 300˚C for 2 h as a function of heating rate (left Figures = 2˚C/min, right Figures = 5˚C/min) and coating thickness (upper Figures = 4 coating layers ≈ 200 nm, lower Figures = 8 coating layers ≈ 400 nm)

Samples heated at soak temperature of 400˚C all show extensive coating. Also, the 'fragments' or 'flakes' of coating appear to have shrunk somewhat as evidenced by the gaps between them. As can be seen, the amount of cracks in coatings tended to increase with increasing heating rate and coating thickness.

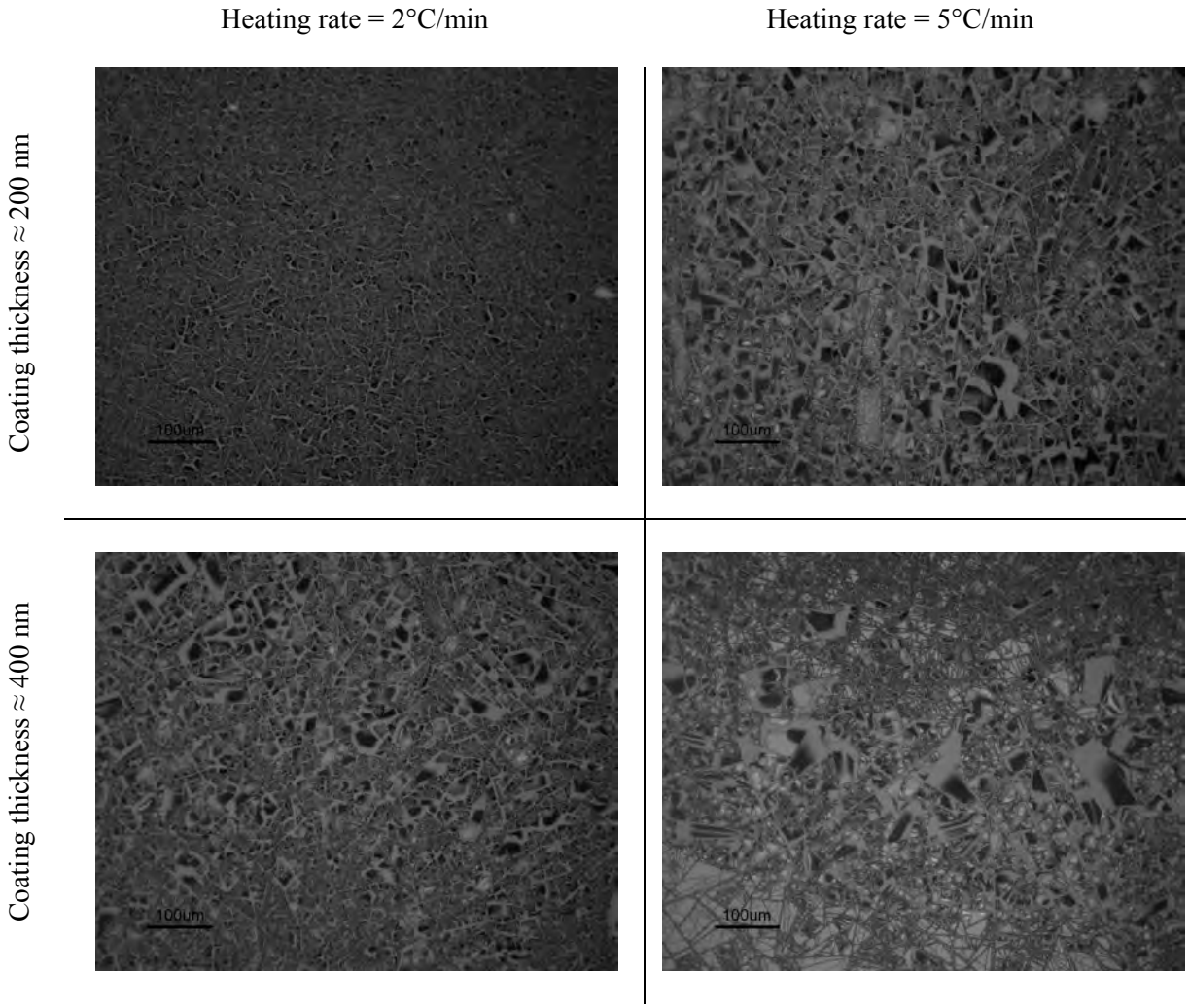

Fig. 5.5 Sol-gel Ga_2O_3 thin film, Type-II sol, on glass substrate, produced by heating at 400˚C for 2 h as a function of heating rate (left Figures = 2˚C/min, right Figures = 5˚C/min) and coating thickness (upper Figures = 4 coating layers ≈ 200 nm, lower Figures = 8 coating layers ≈ 400 nm)

With increasing the soak temperature to 500˚C (Fig. 5.6), the Ga_2O_3 crystals are formed (as XRD data presented later in this section). The formation of these crystals which are type α of Ga_2O_3, characterised by XRD, is not homogeneous and uniform, and noticeable amount of cracks are observable in the final coatings.

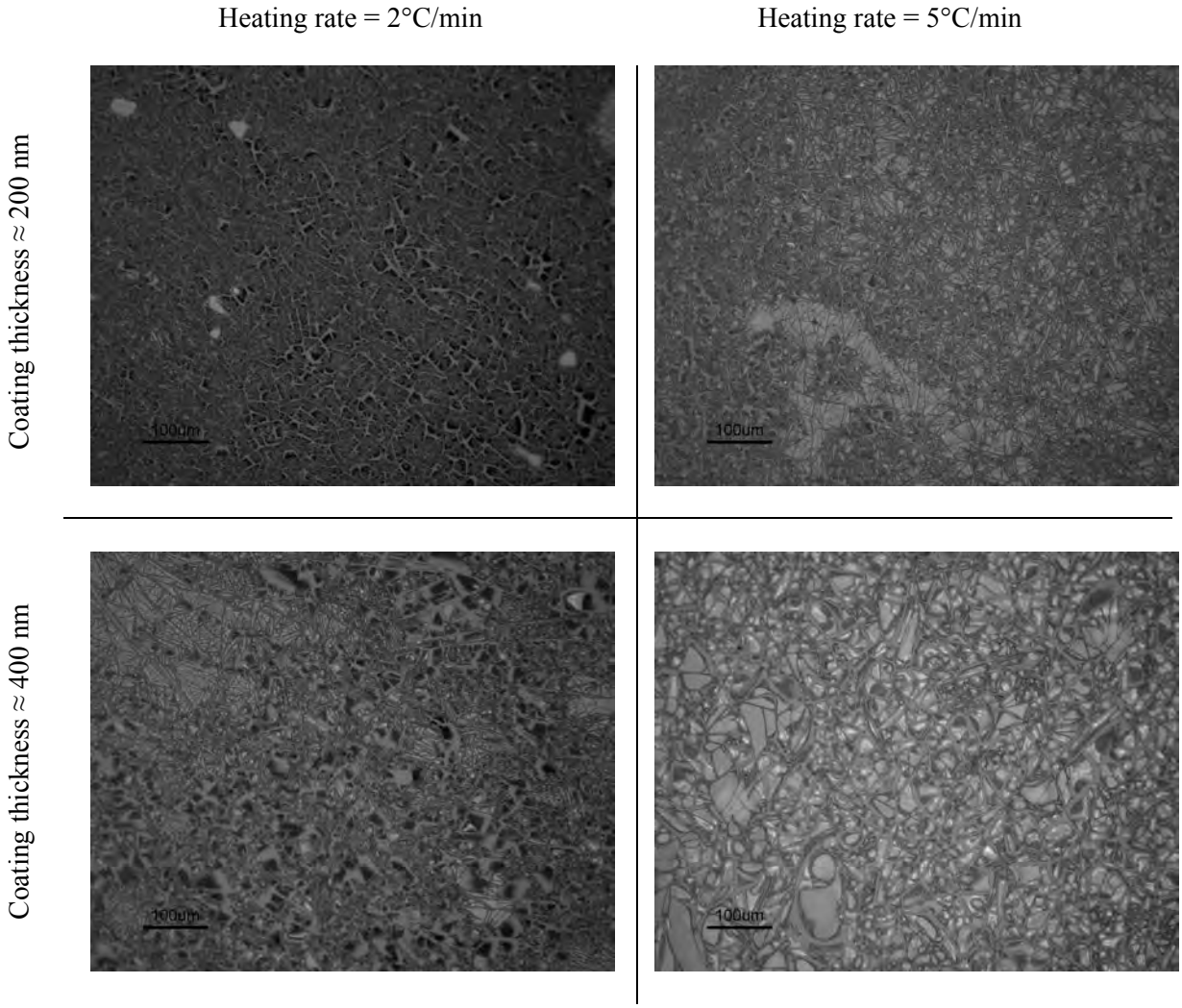

Fig. 5.6 Sol-gel Ga_2O_3 thin film, Type-II sol, on glass substrate, produced by heating at 500˚C for 2 h as a function of heating rate (left Figures = 2˚C/min, right Figures = 5˚C/min) and coating thickness (upper Figures = 4 coating layers ≈ 200 nm, lower Figures = 8 coating layers ≈ 400 nm)

From the above Figures, it is apparent that the coatings experienced a significant amount of cracking at each temperature for the 200 and 400 nm coating thicknesses.

A series of thinner coatings were prepared from the Type-II sol using the slower heating rate of 2˚C/min and thicknesses of ≈ 50 nm (one layer) and ≈ 100 nm (two layers). Compared with the 200 and 400 nm thick coatings, the 100 nm thick coating was much less cracked and the 50 nm thick coating was crack-free.

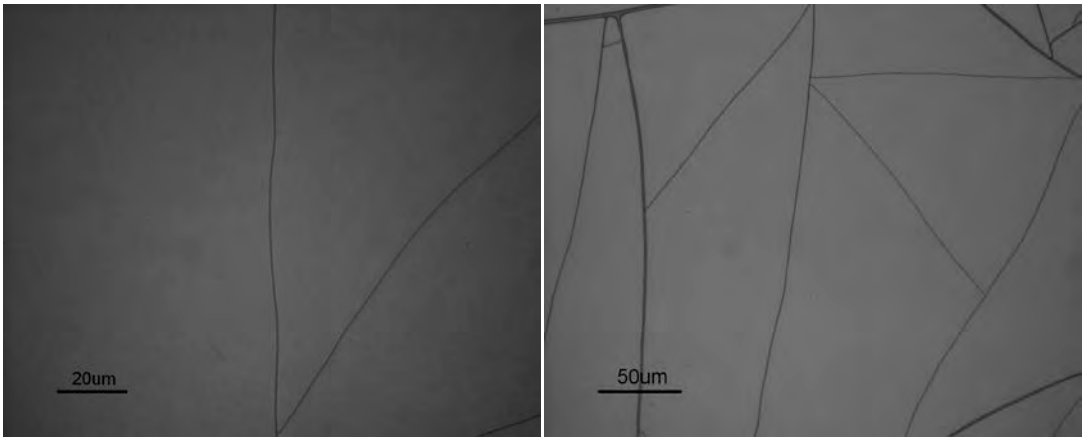

(a)

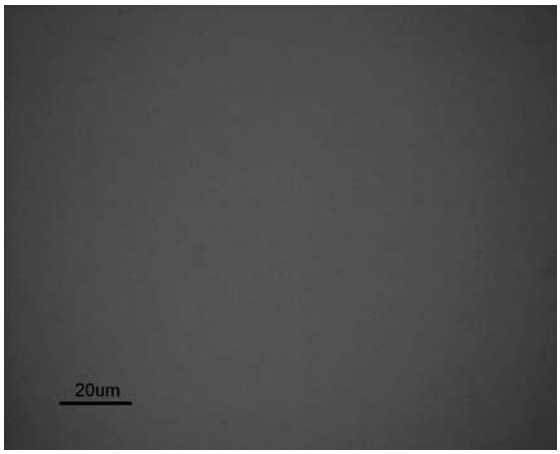

(b)

Fig. 5.7 Type-II sol-gel Ga_2O_3 thin film on glass substrate heated at 500˚C for 2 h using a heating rate of 2˚C/min: (a) 2 spin-coating layers (thickness of coating is 100 nm), (b) one spin-coating layer (thickness of coating is 50 nm).

From optical microscope images, it can be concluded that Type-I sol is not a satisfactory solution because it cannot form a gel in short time. Also, to have a free-crack Ga_2O_3 thin film, heat-treatment conditions such as heating rate and time are key factors. With decreasing the heating rate, the amount of crack in samples decreases considerably. Since the glass substrate cannot tolerate the temperature over 500˚C, quartz (α-quartz) was used as substrate for coating heated above this temperature.

5.2.2 Examination by SEM

SEM was used to examine the morphology of coatings at magnifications higher than those possible with optical microscopy. SEM images of Ga_2O_3 thin films (approximately 200 nm thick) deposited from Type-II sol and heat-treated as a function of heating rate and temperature are shown in Figures 5.8 and 5.9 for glass and quartz substrates, respectively.

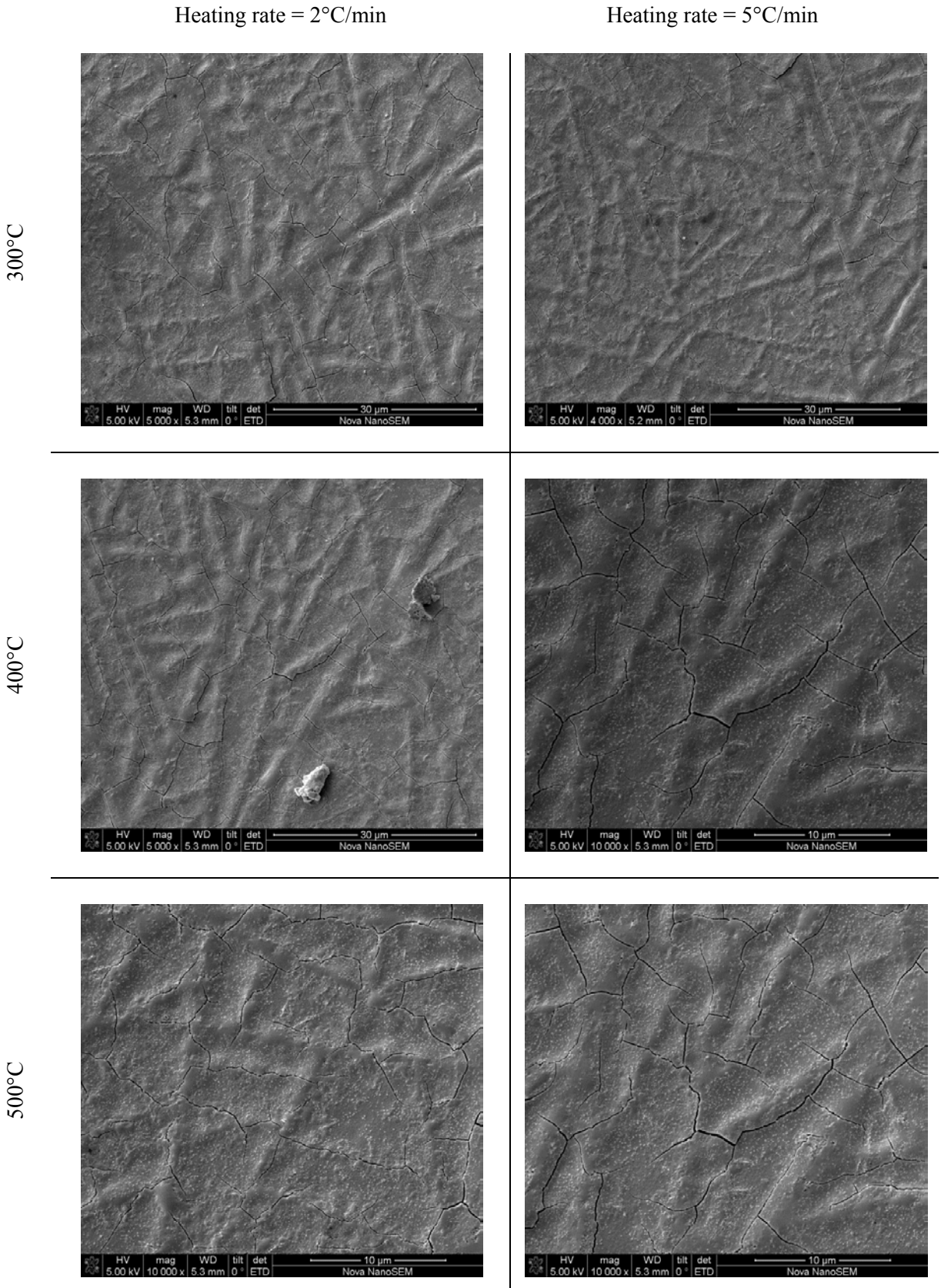

Fig. 5.8 Sol-gel Ga_2O_3 thin film, prepared from Type-II sol on glass substrate, varied heating rate and heating temperature, 4 spin-coating layers (coating thickness ≈ 200 nm)

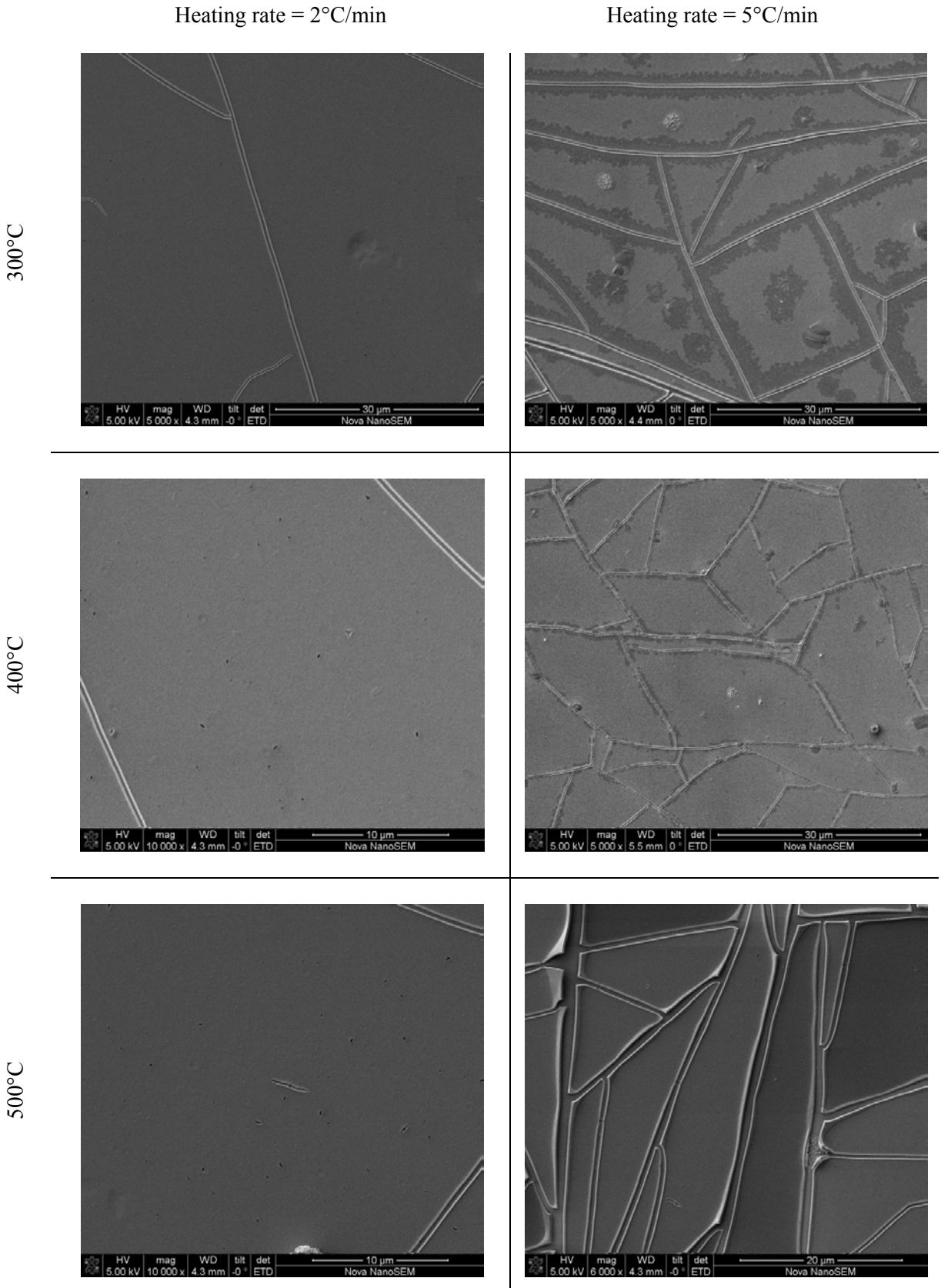

Fig. 5.9 Sol-gel Ga_2O_3 thin film, prepared from Type-II sol on quartz substrate, as a function of heating rate and heating temperature, 4 spin-coating layers (coating thickness ≈ 200 nm).

In general, the coatings on the glass substrates contain a significant amount of cracking and the surfaces appear rough and distorted, the latter manifesting as obvious "ripples" in the surface. The cracks tend to be randomly orientated and intersect each other of at distances of approximately 5 µm. The ripples also appear to be randomly orientated and are approximately a few microns wide. The locations of the ripples do not seem to bear any relationship to those of the cracks. Despite the cracking and apparent roughness, the coatings appear to be well bonded to the glass substrate as evidenced by the lack of any apparent spalling or delamination. Given that the coatings are only ~200 nm thick, the ripples thus are interpreted as being in the coating and substrate together.

The coatings on the quartz substrates show some cracking but, unlike the glass substrates, there are no ripples or distortion of the surface. Compared with the glass substrate, the extent of cracking is noticeably less on the quartz and the cracks tend to be spaced much wider apart (~30 µm and greater) and are straighter. The effect of heating rate was more pronounced in that the faster heating rate produced significantly more cracks. The amount of cracking increased with heat-treatment temperature as did the width of the cracks (thus revealing the substrate below). At the highest temperature of 500°C, the coating at the edges of the cracks appears to have delaminated from the substrate.

The cause of the cracking for both substrate types and the apparent distortion of the glass substrates are interpreted in terms of the thermal mismatch between the Ga_2O_3 coating and the substrate and the resultant stresses generated between the coating and the substrate during heat-treatment and subsequent cooling. This is explained in detail in Section 6.2.

To evaluate the change in main elements' content in coating, EDS analysis using SEM was performed (Fig. 5.10). This analysis was carried out at least five times at different spots for each sample to obtain an average value and the results were the same as shown in Fig. 5.10. The Ga content compared to O, Au and Si content for resulting is given in this figure (Fig. 5.10). Using this analysis it can be shown that the amount of Ga after firing uniformly is constant in comparison to oxygen.

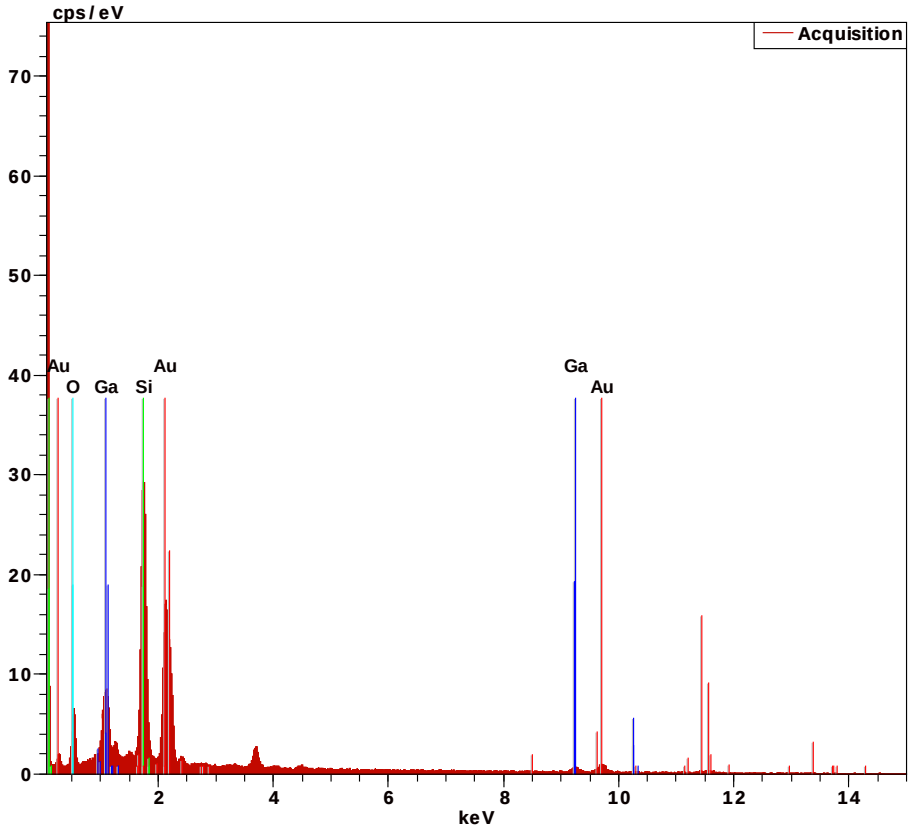

Fig. 5.10 EDS analysis of Sol-gel Ga_2O_3 thin film

5.3 PHASE COMPOSITION

Fig. 5.11 – 5.12 shows the XRD pattern of Ga_2O_3 coating prepared with sol Type-II. It was noted that Ga_2O_3(α, β) basically can be prepared at high temperature (over 500˚C) as reported in recent studies[27, 65]. The crystalline phases in the investigated samples were identified according to the data contained in the ICDD Powder Diffraction File.

A selected thin film XRD pattern of Ga_2O_3 coating on Quartz substrate which have been heat-treated at different temperatures (over 300°C) for 3 h are shown in Fig. 5.11. Quartz was identified as the major phase in all samples. So the diffraction intensity of Ga_2O_3 phases is much lower than that of substrates while the intensity of the substrate peaks remained constant. Using these patterns we are not able to characterize the coatings.

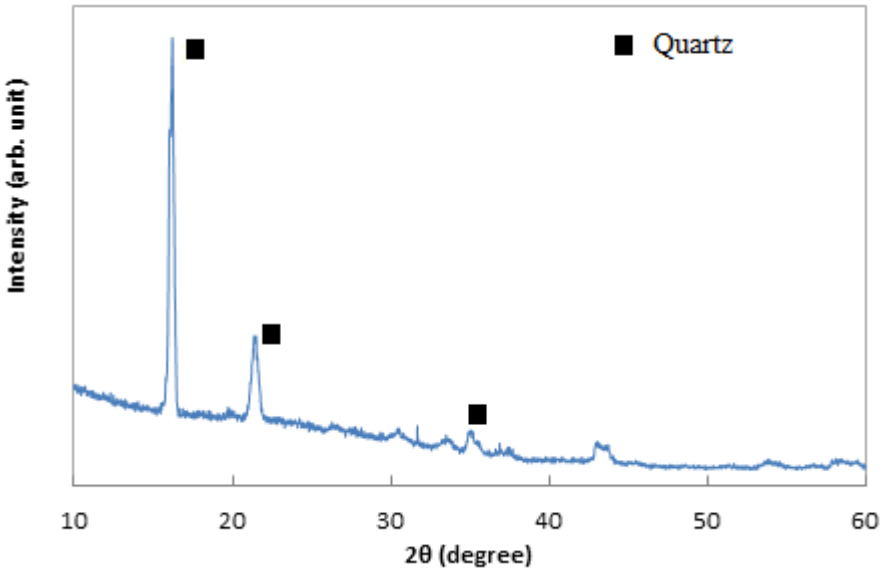

Fig. 5.11 XRD pattern of Ga_2O_3 thin film on quartz substrate

Precursor Ga_2O_3 phases below 300°C in the thin film XRD results were not apparent, because their different peaks are inherently low intensity, not being able to be discerned from the relatively noisy background. Due to their relatively low intensity, the thin film XRD patterns were unsuitable for qualitative analysis of the Ga_2O_3 phases.

The investigation of phase evolution in the coatings, independent of substrate, was examined by X-ray powder diffraction pattern of coatings as a function of temperature. The diffraction patterns are shown in Fig. 5.12. It can be seen that coatings are essentially amorphous up to ~300°C as indicated by the lack of any significant diffraction peaks and the amorphous "hump" between 30° and 40° 2θ. There are some very weak peaks, barely discernable above the background radiation, but which can be ascribed possibly to α-Ga_2O_3. On further heating to 500°C, α-Ga_2O_3 peaks are clearly discernable, albeit relatively weak and broad. At 900°C, the only peaks that are present are due to β-Ga_2O_3 indicating that the α-Ga_2O_3 has fully transformed into β-Ga_2O_3. Also, the 900°C pattern shows well-defined sharp peaks is β-Ga_2O_3 indicating that the coating is well crystallised. These observations are consistent with the phase transformation sequence for pure Ga_2O_3 reported in the literature [13,16]. As explained in Chapter 2, complete crystallization of Ga_2O_3 requires temperatures above 870°C. Therefore, the presence of some amorphous material in the as-prepared coatings and in coatings prepared at 300 and 500°C is consistent with this, as is the obtainment of 100% β-Ga_2O_3 at 900°C.

Accurate determination of the lattice parameters of the Ga_2O_3 phases from the XRD patterns in Fig 5.12 was not possible for several reasons. Firstly, reliable determination of lattice parameters requires an internal standard to calibrate the

goniometer angles of the diffraction peaks. However, it is not technically feasible to include a calibration standard into a (sol-gel) coating. Secondly, the diffraction peaks need to be strong and sharp to enable accurate measurement of their angles. For the XRD patterns shown in Fig. 5.12, strong diffraction peaks occur only for the 900°C diffraction pattern and, whilst it may be possible to measure the peak angles to thus calculate the lattice parameters (of the β-Ga_2O_3 phase), the lack of an internal standard would give questionable reliability of the values obtained. For the XRD patterns obtained for coatings fired at lower temperatures, the lack of strong diffraction peaks means that diffraction angles and hence lattice parameters cannot be determined at all. Thus, ultimately, any effect of firing temperature on lattice parameters cannot be made.

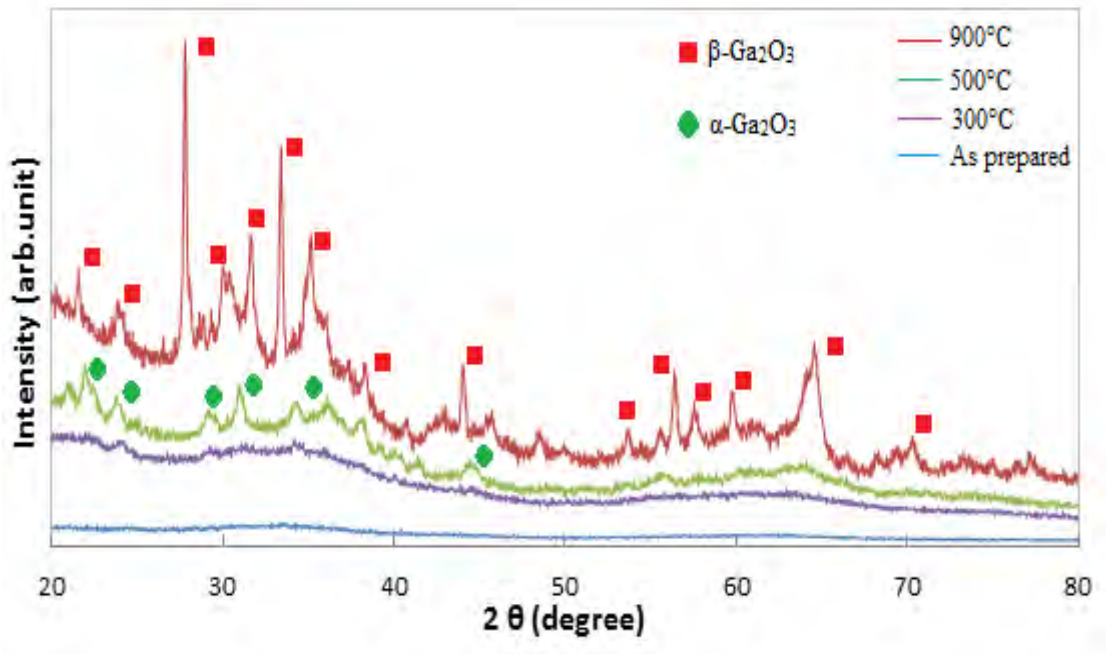

Fig. 5.12 Characteristic parts of X-ray powder diffraction patterns of samples of as-prepared sol-gel and as a function of heat-treatment of a soak temperatures of 300, 500, 900°C (constant heating rate of 2°C/min)

5.4 BANDGAP

The optical bandgap of pure β-Ga_2O_3, Zn3%-doped β-Ga_2O_3, and Zn6%-doped β-Ga_2O_3 coatings was measured by reflective spectroscopy in the spectral range of 300-800 nm as detailed in Section 4.5.4. Plots of reflection versus wavelength for pure β-Ga_2O_3, Zn3%-doped β-Ga_2O_3, and Zn6%-doped β-Ga_2O_3 are given in figures 5.13 – 5.15. Extrapolation of the initial linear portion of each plot to zero reflectance gives the wavelength (λ) of the corresponding optical bandgap energy for the allowed direct reflection. Extrapolation of the linear portion of each plot gave wavelengths for pure β-Ga_2O_3, Zn3%-doped β-Ga_2O_3, and Zn6%-doped β-Ga_2O_3 of 270 nm, 280 nm, and 450 nm, respectively.

The optical bandgap energy (E_g) is then calculated using Planck's equation:

$$E_g = hc/\lambda$$

where: h = Planck's constant (6.626×10^{-34} kg. $m^2.s^{-1}$)

c = speed of the light (2.998×10^{8} $m.s^{-1}$)

The calculation for pure β-Ga_2O_3 for example (including conversion to eV) is:

$$E_g = hc/\lambda$$

$$= (6.626 \times 10^{-34}\ kg.m^2.s^{-1}) \times (2.998 \times 10^{8}\ m.s^{-1}) / (270 \times 10^{-9}\ m)$$

$$\text{x } (1\ eV/1.602 \text{ x } 10^{-19}\ kg.m^2.s^{-2})$$

$$= 4.50\ eV$$

The same calculation for the Zn3%-doped β-Ga_2O_3 and Zn6%-doped β-Ga_2O_3 coatings returned optical bandgap values of 4.42 eV and 2.75 eV, respectively. As explained in Section 4.5.4, the optical bandgap of almost all semiconductors can be taken to be identical to the electronic bandgap. This is true for Ga_2O_3 and thus the optical bandgap values determined above were considered to be reliable values of the electronic bandgap for the pure and doped β-Ga_2O_3 coatings.

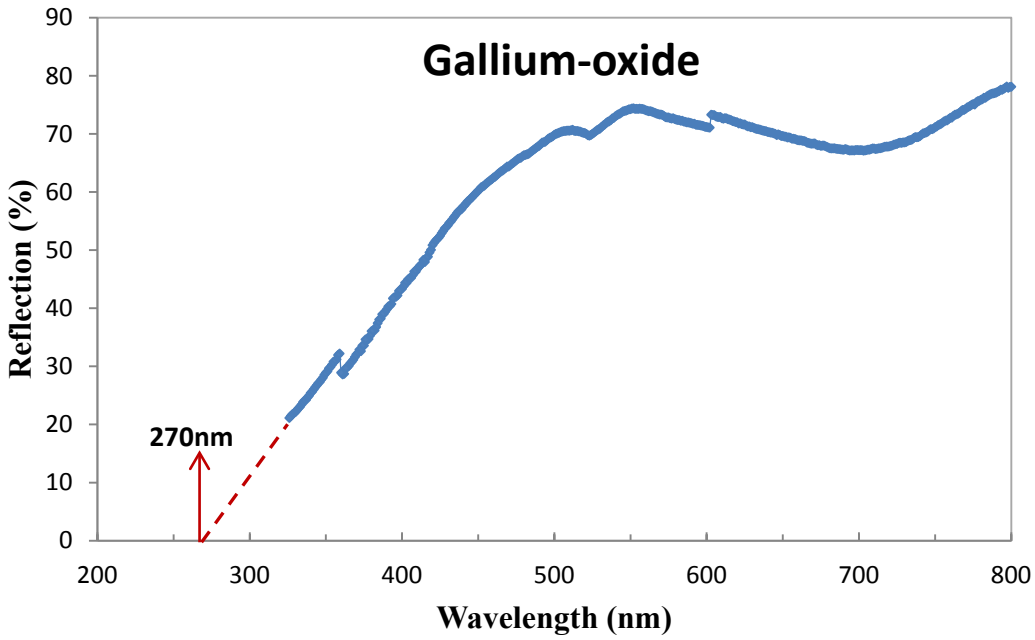

Fig. 5.13 Reflection vs. wavelength plot for pure Ga_2O_3

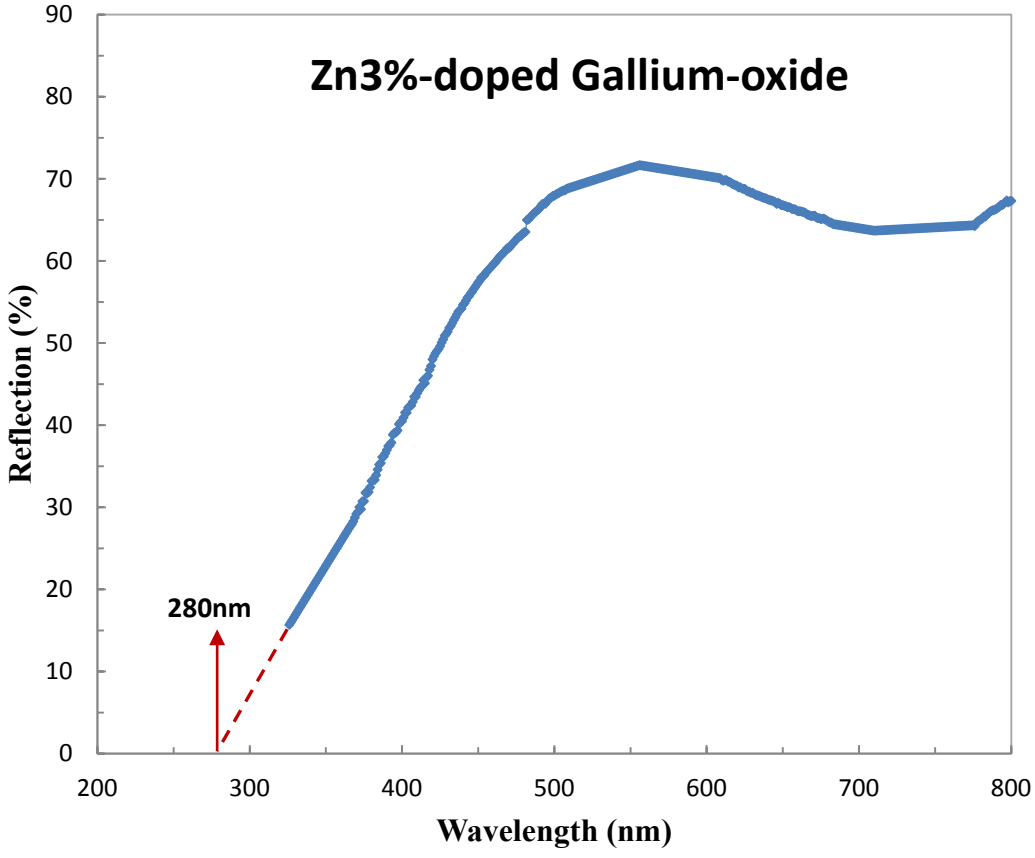

Fig. 5.14 Reflection vs. wavelength plot for Zn3%-doped Ga_2O_3

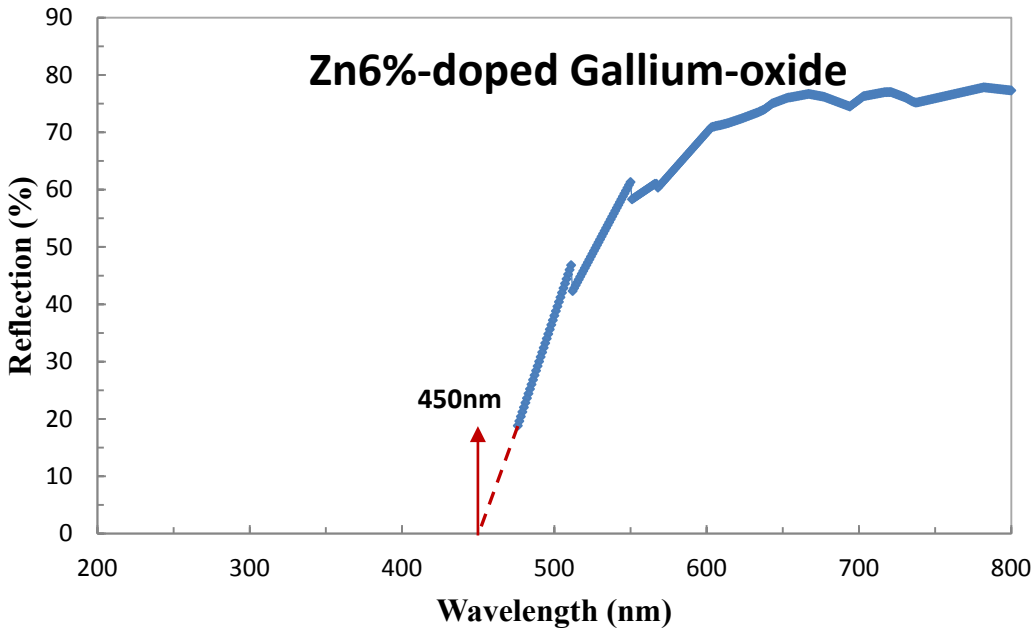

Fig. 5.15 Reflection vs. wavelength plot for Zn6%-doped Ga_2O_3

6. Discussion

6.1 SOL-GEL DEPOSITION PROCESS

Two types of sols were prepared in this work using gallium isopropoxide as the starting precursor. The first sol (Type I sol) was prepared via a aqueous route based on the method developed by Yoldas for alumina sol-gel coatings. The other sol (Type II sol) was prepared via a non-aqueous route involving 2-methoxyethanol (MOE) as the solvent. The Type I sol did not gelate during the deposition process as evidenced by the lack of any visible coating on the substrates examined by optical microscopy (refer to Fig. 5.3). In contrast, the Type II sol produced obvious coatings, albeit with varying extent of cracking depending on the deposition and heat-treatment conditions. The viscometry results (refer to Figure 5.1) show that the Type II sol exhibited a pronounced and continued increase in viscosity after ~60 mins and this is attributed to gelation of the sol. The viscosity of the Type I sol on

the other hand did not show any significant increase even after ~3 hours and instead the sol remained highly fluid suggesting that gelation did not occur. It is likely that during spin coating deposition of the Type I sol the lack of gelation would result in the sol being simply spun off the substrate thus resulting in the absence of any discernible coating. Even if sol was present on the substrate following deposition it is likely that the water would have evaporated very quickly on subsequent drying thus precluding any gelation.

The lack of any obvious gelation in the Type I sol versus gelation in the Type II sol can be considered in terms of the solvation of the gallium isopropoxide precursor in the solvents of water and 2-methoxyethanol, respectively, and the effect on reaction rates. In dissolving process the free energy change of solvent is very important. Since in the chemical reaction of sol-gel Ga_2O_3 using gallium isopropoxide with MOE or water, the ionization equilibrium of an acid or a base is affected by a solvent change, it needs to be considered in this process. Besides this theory, the effect of the solvent could be because of its dielectric constant and its ability to preferentially solvate. A change in the solvating ability or dielectric constant can influence the acidity or basicity. From table 2.3, dielectric constant of water at temperature of 25˚C is about 5 times more than MOE. Therefore, water is more polar-solvent and ionization in water is greater than MOE. Based on the practical experiment, it seems that these characteristic of water has made it as a solvent which is not suitable for Ga-based precursor, it is a proper solvent for Al-based precursor though. It might be due to the difference in the evaporation rate of water compared to MOE. On the other hand, solvents can actually influence reaction rates and order of a chemical reaction and this is in agreement with what can be

shown from the result of viscometry in Figure 5.1. The Type I sol is not considered hereafter since it was not capable of depositing a coating.

6.2 EFFECT OF COATING THICKNESS, HEAT TREATMENT CONDITIONS, AND SUBSTRATE TYPE ON COATING STRUCTURAL EVOLUTION

The effects of the coating thickness, heat treatment conditions (heating rate and soak temperature), and substrate type on coating formation and evolution of phase composition and microstructure are now discussed for the Type II sol. During spin coating, the Type II sol was able to spread out uniformly on the surface of substrate (glass) and to gelate to form a coherent coating. Subsequent heat treatment at 300°C for 2 hours produced transparent coatings containing a network of fine cracks (see Figure 5.4 for coatings on glass substrates). The amount of cracking tended to increase with increasing heating rate (from 2 to 5°C /min) and with increasing coating thickness (from 200 to 400 nm). It would be expected that during heating up to 300°C and then holding at this temperature, any residual solvent in the gelated coating would evaporate causing shrinkage of the coating. Moreover, it is likely that the evaporation of solvent at the coating surface would be faster than the rate of diffusion of solvent through the coating thereby establishing a concentration gradient of the solvent between the coating surface (lowest concentration) and the substrate (highest concentration). Concomitant with the establishment of this concentration gradient would be a differential in the shrinkage of the coating across its thickness in that the highest shrinkage would be at the coating surface and the lowest shrinkage would be at the coating-substrate interface. This differential shrinkage would result in the coating surface being placed into a state of tension

which, if exceeding the inherent tensile strength of the gelated coating, would cause cracking. The effects of heating rate and coating thickness can now be explained.

Increasing the heating rate should increase the rate of evaporation of solvent from the coating surface to a greater extent than the rate of solvent diffusion through the coating. This would increase, in turn, the magnitudes of the solvent concentration gradient, the differential shrinkage, and the tensile stress at the coating surface thus, ultimately, resulting in more extensive cracking of the coating. As can be seen in Figure 5.4, the coatings heated at the faster heating rate of 5°C/min had a finer network of cracks compared with the coatings heated at 2°C/min. Although not tested in this work, it is anticipated that using slower heating rates than 2 °C/min should decrease the incidence of cracking.

Increasing the coating thickness increases the distance through which the solvent must diffuse to the surface or, in other words, increases the magnitude of the solvent concentration gradient. This increases the differential shrinkage and thus the tensile stress at the coating surface and ultimately increasing the extent of cracking in the coating. As can be seen in Figure 5.4, the ~400 nm thick coatings were noticeably more cracked than the ~200 nm thick coatings. Obviously, decreasing the coating thickness (by control of the sol-gel deposition process) should decrease the incidence of cracking by decreasing the solvent diffusion distance through the coating. In addition, as the coating gets thinner, the lateral shrinkage of the coating becomes more restrained by whatever interfacial bonding between the coating and the substrate. As a result, the coating tends to shrink "downwards" onto the substrate such that the lateral tensile stresses are reduced which, in turn, reducing the tendency of the coating to crack. As shown in Figure 5.7 (for Type II sol-gel coating heat treated at 500°C using a heating rate of 2°C/min), reducing the coating thickness to

100 nm greatly reduced the amount of cracking in the coating and further reducing the thickness to 50 nm resulted in crack-free coatings.

In the micrographs shown in Figure 5.4, it is apparent that there are instances of where multiple cracks emanate from specific points in the coatings. It is speculated that these points may be minute defects in the coating such as bubbles or particulate inclusions (e.g. from dust) and that these defects act as initiation sites for crack propagation when the coating surface is placed into a state of tension.

Heat treatment of the coatings at 400 and 500°C (Figures 5.4 and 5.6, respectively) resulted in the already cracked coatings undergoing further cracking and, in addition, significant shrinkage of the coating "flakes". The shrinkage is attributed to the loss of mass that would have occurred during the pyrolysis of the organic phase and also to the onset of sintering and densification of the resultant gallium oxide. Furthermore, it is apparent that there are areas of the coating in which the coating has delaminated and spalled from the substrate. The cracking, shrinkage, delamination, and spalling collectively result in a significant decrease in the "quality" of the coating. Obviously, such coatings would not be suitable for any engineering or electronic applications. By decreasing the coating thickness, the above firing shrinkage tends to become restrained in the lateral directions (again, by virtue of whatever interfacial bonding) such that the coating tends to shrink "downwards" onto the substrate thereby reducing the tendency of the coating to crack. Coatings of Type II sol on glass heat treated at 500°C (using a heating rate of 2°C/min) were crack-free at a thickness of 50 nm.

It is apparent from SEM images of the coatings on glass (Fig. 5.8) that there are "ripples" in the coated substrate. The glass is a relatively low-temperature soda-lime-silicate glass (used for microscope slides) and it is possible that the glass has

softened at temperatures of ≥300°C such that the compressive stress induced by the shrinking coating has effectively "pulled" the glass surface together thus creating the "ripples". Also, the coefficient of thermal expansion of the glass (~8-9 x 10^{-6} $°C^{-1}$) is significantly less than that of the Ga_2O_3 coating such that the differential thermal contraction on cooling from ~300°C would result in the coating tending to exert a tensile stress in the glass near the glass surface. Given that the glass is relatively less stiff (Young's modulus ~ 70 G Pa) than the coating, this tensile stress could be relieved by the glass deforming or "rippling" at the surface.

The above "rippling" effect was not observed when quartz was used as the substrate which is reasonable since quartz would not be expected to soften much before its melting point. The coatings on the quartz substrates showed similar behaviour to those on the glass substrates in that the extent of cracking tended to decrease with decreasing heat rate (from 4 to 2 °C/min) as shown in Fig. 5.9. However, compared with the coatings on glass substrates, the coatings on quartz substrates were significantly less cracked at all heat treatment temperatures. This is attributed to two effects. Firstly, it is possible that the adherence of the sol-gel coating was stronger on the quartz than on the glass because of more crystallographic lattice match between coating and quartz substrate compared to coating and glass substrate, thereby making the coating more resistant to cracking and delamination during shrinkage. Secondly, the thermal expansion coefficient of the quartz is likely to be smaller than the glass such that differential expansion/contraction between the coating and the substrate on heating/cooling is likely to be less for quartz compared with glass, thus resulting in less cracking.

6.3 EFFECT OF HEAT TREATMENT CONDITIONS ON COATING STRUCTURAL EVOLUTION

To characterise the phase evolution of sol-gel Ga_2O_3 coating, a selected thin film XRD pattern of Ga_2O_3 coating on Quartz substrates which have been heat-treated at different temperatures (300 - 900°C) for 3 h are shown in Fig. 5.11 and 5.12.

The XRD pattern showed that coatings are essentially amorphous before heating to 300°C (Fig. 5.12). And the peaks would start to show after 500°C.

When samples heated at 500°C, it remained dominantly amorphous, but showed faint diffraction lines of α-Ga_2O_3 and β-Ga_2O_3 which has been reported[27]. The same sample, upon heating at 900°C, was β-Ga_2O_3 with broadened diffraction lines. The Ga_2O_3 phase in the pattern was β-Ga_2O_3 and the diffraction intensity of this phase was always much lower than that of substrates. The intensity of β-Ga_2O_3 peaks tended to increase with increasing heat treatment temperature and time while the intensity of the substrate peaks remained constant.

The broadening of XRD lines of the crystalline phases depended on the Miller indices, thus indicating anisotropic shapes of crystallites. The results of XRD analysis showed a strong dependence of the phase composition of the samples on the experimental conditions of their preparation. On the other hand, Gallium isopropoxide dissolved in MOE (Type-II sol) would result in a completely amorphous phase, which upon heating at 900°C gave β-Ga_2O_3 as a single phase.

6.4 EFFECT OF DOPANTS ON SOL-GEL Ga_2O_3 COATING

Table 4.1 shows that Ga^{3+} is close to Zn^{2+}, Mn^{2+}, and Cu^{2+} in terms of ionic and covalent radius. Thus these ions could be potential ions as dopants for Ga^{3+} based on what was explained in section 4.3.2. It supposed that making solution of these ions with Ga^{3+} using sol-gel technique would be easily possible. However, it was possible practically only for Cu^{2+} solution could react with gallium oxide sol and result in a homogenous solution. The reaction of other ions with gallium-base precursor led to precipitated solutions as indicated in Table 6.1.

Table 6.1 Final solution of precursors and dopants (electronegativity values are indicated in parenthesis)

dopant / precursor	Zn^{2+} (1.65)	Mn^{2+} (1.55)	Cu^{2+} (1.88)
Ga^{3+} (1.81)	P	P	H
Al^{3+} (1.61)	H	H	NH

P=Precipitated
H= Homogenous transparent solution
NH= Non-homogenous solution

To understand what happens in the chemical reaction of Ga-based precursor with other ions, a comparison was performed with aluminium precursor (aluminium butoxide) which is similar to gallium alkoxide. As mentioned gallium and aluminium are in a same group in the periodic table of the elements, and the chemical and physical behaviors of their oxides are generally comparable with each

other in terms of morphology. Besides Ga, the dopant solution of alumina sol with the mentioned ions was made. As can be seen in Fig. 6.1, the result was interesting when the reaction of Zn^{2+} and Mn^{2+} solution with Al^{3+} were a homogenous solution without any precipitation. Interestingly, the reaction of Cu^{2+} with Al^{3+} was different from Ga^{3+} and was not as homogenous as Ga^{3+}.

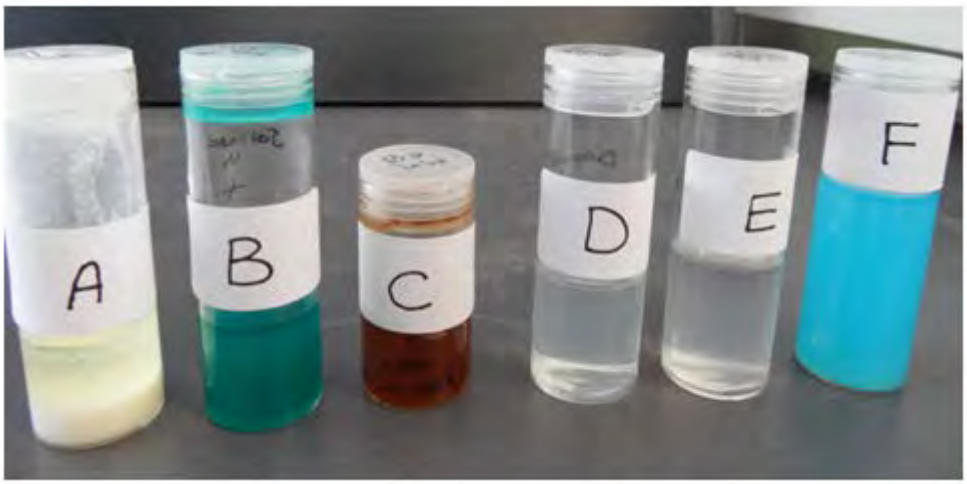

Fig. 6.1 Final solution of precursors and dopants: (A) Zn-doped Ga based precursor, (B) Cu-doped Ga based precursor, (C) Mn-doped Ga based precursor, (D) Zn-doped Al based precursor, (E) Mn-doped Al based precursor, (F) Cu-doped Al based precursor

The results indicate that to find a suitable dopant for Ga-based precursor, electronegativity of cations in compound is an important factor to be considered. Just those dopants could be compatible for this type of precursor that has electronegativity close to Ga^{3+}.

For doping a metal-oxide such as gallium oxide or alumina, the method is considered based on what explained in Fig. 4.3. To make a solution of dopant, the first issue was

technique to make the solution and the reaction of most ions with gallium-base precursor led to a precipitated solution (refer to table 6.1).

From the electronegativity data of elements, it can be shown that aluminium, zinc, and manganese are close to each other while it is almost similar for Gallium and Cupper. That might be the fact that why Ga^{3+} could make a homogenous transparent solution with Cu^{2+} but other ions.

Electronegativity differences drive charge transfers on molecule formation. It is the chemical potential of density functional theory. While energy and not electronegativity determines whether a chemical bond will form, electronegativity differences determine the charge transfers which occur on bond formation. The method used for the preparation of a metal alkoxide depends, in general, on the electronegativity of the metal.

The physical properties of metal alkoxides depend primarily on the characteristics of the metal that one of metal characteristic is its electronegativity besides valence, atomic radius, and coordination number. Therefore, as discussed electronegativity of metal in metal alkoxide involving in the chemical reaction plays a big role and should be considered.

6.5 COMPARISON BETWEEN THEORETICAL AND EXPERIMENTAL RESULTS

The effect of doping Ga_2O_3 with Sn^{4+}, Zn^{2+}, and W^{6+} cations was considered by simulation modeling using Material Studio software in Chapter 3 (see Table 3.2). It was shown that doping with increasing amounts of these dopants gave systematic changes in the lattice parameters of β-Ga_2O_3 as well as the electronic bandgap

energy. For the latter, experimental data for one selected dopant (Zn) was determined using reflective spectroscopy (see Section 5.4) thus enabling a comparison of modeled and experimental bandgap energies. The values of modeled and experimental bandgap energies for pure β-Ga_2O_3, Zn3%-doped β-Ga_2O_3, and Zn6%-doped β-Ga_2O_3 coatings are given in Table 6.2 below and are plotted in Figure 6.2.

Table 6.2 Comparison in bandgap energies for pure β-Ga_2O_3, Zn3%-doped β-Ga_2O_3, and Zn6%-doped β-Ga_2O_3 coatings between simulated and experimental work

Sample	Bandgap (eV)	
	Simulation	Experiment
Ga_2O_3	2.32	4.50
Zn3% doped	2.26	4.42
Zn6% doped	1.42	2.75

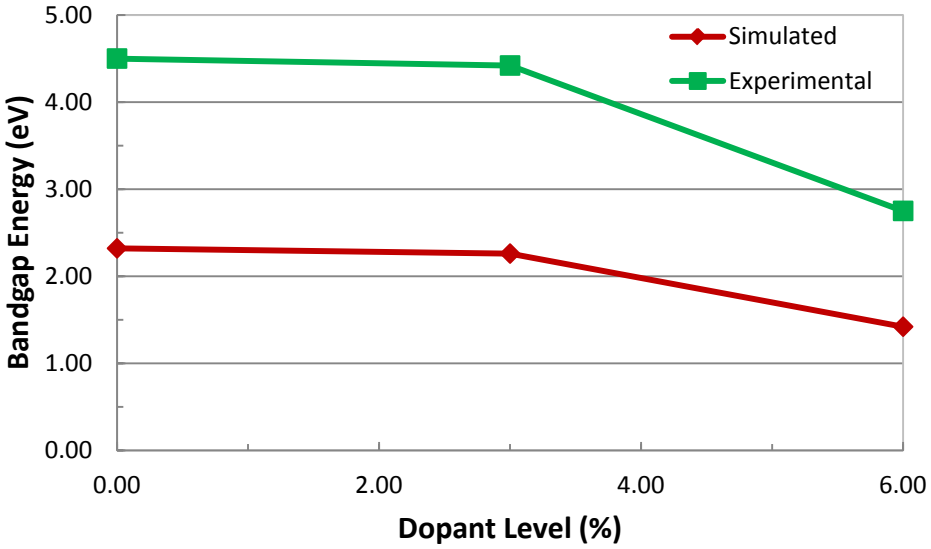

Fig. 6.2 Simulated and experimental bandgap energies for pure β-Ga_2O_3, Zn3%-doped β-Ga_2O_3, and Zn6%-doped β-Ga_2O_3 coatings.

The bandgap data in Table 6.2 and Figure 6.2 show that both the simulated and experimental bandgap energies decrease with increase concentration of Zn-dopant, consistent with the electronic defect model as discussed earlier. However, the bandgap energies obtained by for the experimental coatings are consistently ~2 times higher than the corresponding values obtained by simulation. This disparity is attributed largely to the limitations in the simulation done using Material Studio software. As explained in Chapter 3, this software employs density functional theory (DFT) for total energy to simulate the crystal structure and associated properties. DFT is not able to incorporate all of the factors that contribute to the crystal/electronic structure and typically underestimates the value of the bandgap energy. Notwithstanding this, the software is a useful means of predicting trends in bandgap energy (and other electronic properties) and, in particular for this work, in confirming the effect on bandgap energy by the addition of dopant cations to β-Ga_2O_3.

Better comparison of the simulated and experimental bandgap data is obtained by normalising the values to the respective value for pure β-Ga_2O_3. The resultant data are shown in Figure 6.3. On this basis, the simulated values agree very well with the experimental values. The data show that the bandgap energy of β-Ga_2O_3 is reduced by ~40% by the addition of 6% Zn cations. This indicates that the defect model used in the simulation is reasonable and in agreement with that indicated in the literature.

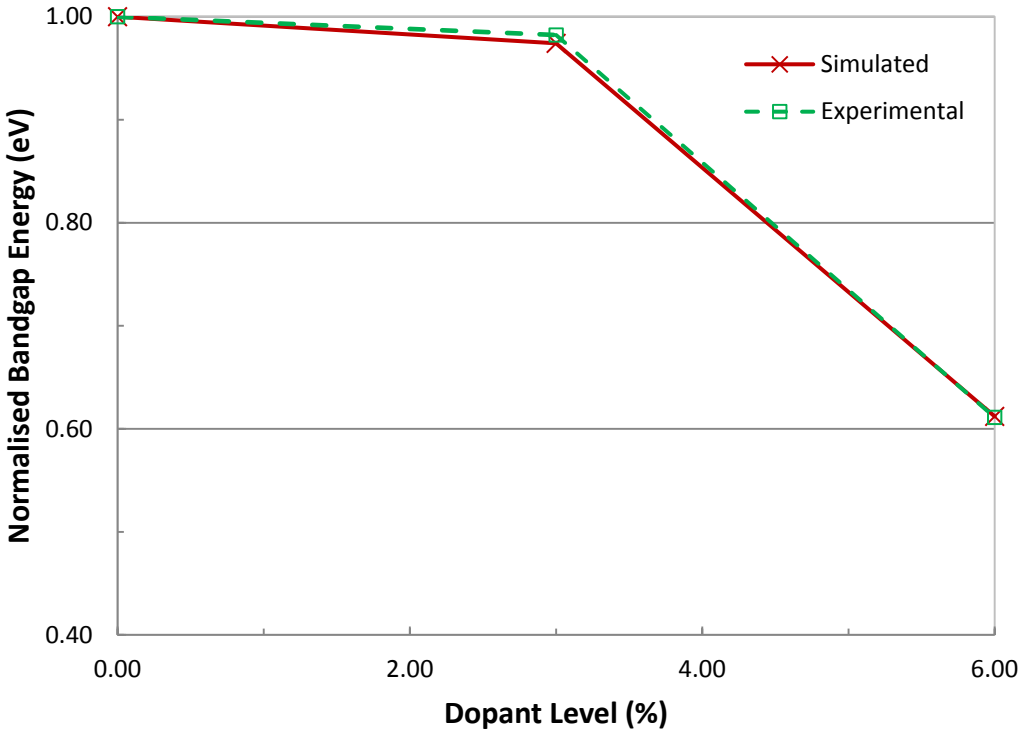

Fig. 6.3 Normalised si mulated an d ex perimental b andgap en ergies f or pure β-Ga_2O_3, Zn3%-doped β-Ga_2O_3, and Zn6%-doped β-Ga_2O_3 coatings. Values are normalised to the respective values for pure β-Ga_2O_3.

7. Conclusion

The overall aim of this thesis was to develop a sol-gel synthesis route for the deposition of pure and doped gallium oxide (Ga_2O_3) coatings, to study the phase evolution in the coatings as a function of coating thickness and heat treatment time. Related to this was the aim to evaluate theoretically the crystal structure and electrical properties of coating doped with different percentages of various dopant ions by simulation and modelling of the intrinsic- and doped-Ga_2O_3 structures using Materials Studio software, and to compare the theoretical results with experimental data.

In order to accomplish the aims of this work specified in chapter 1, the study was divided into the four (4) sequential stages of experimental work.

To develop Ga_2O_3 coating, two types of sols were prepared in this work using gallium isopropoxide as the starting precursor. The first sol (Type-I sol) was

prepared via an aqueous route based on the method developed by Yoldas for alumina sol-gel coatings. The other sol (Type-II sol) was prepared via a non-aqueous route involving 2-methoxyethanol (MOE) as the solvent. The principle of coating process was the deposition of these sols onto substrate (glass and quartz) by spin coating followed by drying and then heat treating at elevated temperature. The Type-I sol did not gelate during the deposition process as evidenced by the lack of any visible coating on the substrates. In contrast, the Type-II sol produced obvious coatings, albeit with varying extent of cracking depending on the deposition and heat-treatment conditions. The lack of any obvious gelation in the Type-I sol versus gelation in the Type-II sol was considered in terms of the solvation of the gallium isopropoxide precursor in the solvents of water and 2-methoxyethanol, respectively, and the effect on reaction rates.

The effects of the coating thickness, heat treatment conditions (temperature and heating rate), and substrate type on the conversion of the initial gallium-oxide precursor (sol) to β-Ga_2O_3 and the corresponding evolution of microstructure were studied. The initial deposited phase of gallium oxide transformed to α-Ga_2O_3 and then to β-Ga_2O_3 with increasing temperature. At 500°C, α-Ga_2O_3 phase started to form and by 900°C, β-Ga_2O_3 was only stable phase of gallium oxide. Heat treatment (for 2 h) at different temperatures affected the coating behaviour in terms of the amount of cracking. The amount of cracking tended to increase with increasing heating rate and with increasing coating thickness. Increasing the heating rate in heat-treatment of coating led to more extensive cracking of the coating. This was mainly due to increase the rate of evaporation of solvent from the coating surface to a greater extent than the rate of solvent diffusion through the coating. The choice of substrates for Ga_2O_3 was studied since it is critical and substantial for making high-

quality coatings. This study showed that quartz could be a compatible substrate for gallium oxide coating.

In this work, the effect of adding different dopants on the electrical properties of gallium oxide coatings were investigated theoretically using proprietary software called Materials Studio. The modeling of Ga_2O_3 showed that the introduction of the Sn and Zn caused the impurity energy level at the bottom of the conduction band. Therefore, the conductivity of the Zn-doped and Sn-doped β-$Ga_2O_3$was improved compared to the intrinsic β-Ga_2O_3.Also, the introduction of Sn and Zn to Ga_2O with Also, to investigate which ions could be suitable as dopant for Ga^{3+} in terms of sol-gel process, doping solution of these ions with Ga^{3+} were made. Our study showed that to find compatible ions as dopants for Ga^{3+}, electronegativity of cations are a key factor. Just those dopants could be compatible for this type of precursor that has electronegativity close to Ga^{3+}. This ion (Ga^{3+}) could make a homogenous transparent solution just with Cu^{2+} but other ions and this showed that the basic theory about electronegativity is an important consideration in developing sol-gel routes for doped-gallia, and doped-oxides in general.

The optical bandgap energy was determined experimentally for sol-gel produced coatings of pure β-Ga_2O_3, Zn3%-doped Ga_2O_3, and Zn6%-doped Ga_2O_3. Like the simulated values, the experimental values decreased with increasing Zn dopant amount thus suggesting that the structural model used to simulate the Ga_2O_3 and the role of dopants in the electronic bandgap structure were fundamentally correct. The structural model and the bandgap data indicate that the β-Ga_2O_3 is monoclinic and that the Zn dopants from a substitutional solid solution with the Ga_2O_3. The experimental value of the bandgap energy for pure β-Ga_2O_3 agreed reasonably well with values reported in the literature and the experimental values for the pure and

doped coatings were consistently ~2 times higher than the simulated values which suggested that the structural model used to calculate the bandgap energies systematically underestimated the values. This was attributed to limitations in the structural model. Regardless, the structural model was considered reliable for predicting the effects of dopants on selected structural and electronic properties of Ga_2O_3.

8. Future work

Future work in this field can be carried out in two different directions, firstly by overseeing the new developments in the computational aspects and secondly by following up the results obtained in this thesis in the term of experimental condition. The stable β- Ga_2O_3 phase gallium oxide is formed at temperatures over 870˚C. Seeding with other metal-oxides in the sol-gel process, as done with alumina for example, may be a potential mean of significantly lowering the crystallisation temperature of gallium oxide as well as giving transformation directly to the high temperature β-Ga_2O_3 phase. Also, further work could be done on examining the cross-sectional microstructure of the coatings by TEM to investigate in detail the coating-substrate interface and, in particular, any differences in the bonding characteristics of the coating with the two different substrates of glass and quartz.

9. References

1. Shan, F., Liu, G., Lee, W., Kim, S., *Structural, electrical, and optical properties of transparent gallium oxide thin films grown by plasma-enhanced atomic layer deposition.* Applied Physics, 2005. **98**: pp. 023504- 023510.

2. Hu, J., Li, Q., Meng, X., Lee, C., Lee, S., *Synthesis of β-Ga_2O_3 nanowires by laser ablation.* Phys. Chem. B, 2002. **106**: pp. 9536–9539.

3. Passlack, M., Schubert, E., Hobson, W., Hong, M., Moriya, N., Chu, S., Konstadinidis, K., Mannaerts, J., Schnoes, M., and Zydzik, G., *Ga_2O_3 films for electronic and optoelectronic applications.* Journal of Applied Physics, 1995. **77**: pp. 686-693.

4. Li, Z., Moodera, J., *Gallium oxide as an insulating barrier for spin-dependent tunneling junctions.* Applied Physics Letters, 2000. **77**: pp. 3630-3633.

5. Binet, G., *Origin of the blue luminescence of β-Ga_2O_3.* Applied Physics Letters, 1998. **59**: pp. 1241-1249.

6. Fleischer M., *Electron mobility in single and polycrystalline Ga_2O_3.* Applied Physics Letters, 1993. **74B**: pp. 300–305.

7. Ogita, M., Nakanishi, Y., Hatanaka, Y., *Ga_2O_3 thin film for oxygen sensor at high temperature.* Applied Surface Science, 2001. **175**: pp. 721-725.

8. Fleischer, M., *Sensing reducing gases at high temperatures using long-term stable Ga_2O_3 thin films.* Sensors and Actuators, 1992. **6**: pp. 257-261.

9. Fleischer M., *Sensing Gallium oxide thin films: a new material for high-temperature oxygen sensors.* Sensor and Actuators, 1991. **B4**: pp. 437-441.

10. Li, Y., Wlodarski, W., Galatsis, K., Kalanter-Zadeh K., *Investigation of the oxygen gas sensing performance of Ga_2O_3 thin films with different dopants.* Sensors & Actuators, 2003. **B 93**: pp. 431-434.

11. Ueda, N., Waseda, R., Kawazoe, H., *Anisotropy of electrical and optical properties in β-Ga_2O_3.* Applied Physics Letters, 1997. **71**: pp. 933-935.

12. Hao, J., *Optical and luminescent properties of undoped and rare-earth-doped Ga_2O_3 thin films deposited by spray pyrolysis.* Applied Physics Letters, 2002. **35**: pp. 433-438.

13. Roy R., Osborn, E., *Polymorphism of Ga_2O_3 and the System Ga_2O_3-H_2O.* American Ceramic Society, 1952. **74**: pp. 719-722.

14. Ahman J, Svensson, G., Albertsson, J., *A reinvestigation of β-Ga_2O_3 oxide,* Acta Crystallogr., 1996. **C52**: pp. 1336-1338.

15. Matsuzaki, K., Kamiya, T., *Field-induced current modulation in epitaxial film of deep-ultraviolet transparent oxide semiconductor Ga_2O_3.* Applied Physics Letters, 2006. **88**: pp. 092106(1/3).

16. Qian, H., Zhang, Y., Lin, G., Zheng, J., Xu, R., *Template-free synthesis of highly uniform α-GaOOH spindles and conversion to α- Ga_2O_3 and β-Ga_2O_3.* Crystal Growth, 2008. **8**: pp. 1282–1287.

17. Laubengayar, A., *The sesquioxide and hydroxides of gallium.* American Ceramic Society, 1939. **61**: pp. 1210-1214.

18. Machon, D., Xu, B., Dong, J., *High-pressure study of the α-to β- transition in Ga_2O_3.* Physical rev., 2006. **B 73**: pp.352-363.

19. Yoshioka, S., Kuwabara, A., Oba, F., Matsunaga, K., Tanaka, I., *Structures and energetics of Ga_2O_3 polymorphs.* Physics Condensed Matter, 2007. **19**: pp. 346211-21

20. Fleischer, M., *Characterization and crystallite growth of semiconducting high-temperature-stable Ga_2O_3 thin films.* Materials Science Letters, 1992. **11**: pp. 1728-1731.

21. Battiston, G., Porchia, M., Bertoncello, R., Caccavable, C., *Chemical vapour deposition and characterization of gallium oxide thin films* Thin Solid Films, 1996. **279**: pp. 115-118.

22. Orita, M., Hirano, M., *Deep-ultraviolet transparent conductive β-Ga_2O_3 thin films.* Applied Physics Letters, 2000. **77**: pp. 4166-4168.

23. Fleischer, M., *Thin-film gas sensors based on high-temperature-operated metal oxides.* Vacuum Science and Technology, 1999. **17**: pp. 1866-1872

24. Passlack, M., Mannaerts, J., *Quasistatic and high frequency capacitance–voltage characterization of Ga_2O_3–GaAs structures fabricated by in situ molecular beam epitaxy.* Applied Physics Letters, 1996. **68**: pp. 1099

25. Marie, P., Cardin, J., *Growth and characterization of gallium oxide thin films by radiofrequency magnetron sputtering.* Phys. Stat. Sol., 2008. **205**: pp. 1943–1946.

26. Kokubun, Y., *Sol-gel prepared β-Ga_2O_3 thin films for ultraviolet photodetectors.* Applied Physics Letters, 2007. **90**: pp. 031912-1/3.

27. Ristic, M., Music, S., *Application of sol-gel method in the synthesis of gallium oxide.* Materials Letters, 2004. **59**: pp. 1227-1233.

28. Sinha, G., Chaudhuri, S. , *Sol-gel derived phase pure α-Ga_2O_3 nanocrystalline thin film and its optical properties.* Crystal Growth, 2005. **276**: pp. 204-207.

29. Binions, R ., Carmalt, C ., *Gallium oxide thin films from the atmospheric pressure chemical vapor deposition reaction of gallium trichloride and methanol.* Chemistry and Materials, 2004. **16**: pp. 2489-2493.

30. Aggarwal, S ., Ramesh, R., *Point defect chemistry of metal oxide heterostructures.* Annual Reviews in Materials Science, 1998. **28**: pp. 463-499.

31. Yamaga, M., *Donar structure and electric transport mechanism in β-Ga_2O_3.* Physical Review B, 2003. **68**: pp. 431-443.

32. Wahl, K., Dunn, D., Singer, I., *Effects of ion implantation on microstructure, endurance and wear behavior of IBAD MoS_2.* Wear, 2000. **237**: pp. 1–11.

33. Bae, I., *Phase and microstructural development in alumina sol-gel coatings on CoCr alloy.* Materials Science: Materials in Medicine, 2004. **15**: pp. 959-966.

34. Lange, F ., *Powder processing science and technology for increased reliability.* American Ceramic Society, 1989. **72**: pp. 3-15.

35. Brinker, C., Scherer, G., *Sol-Gel Science: The Physics and Chemistry of Sol-Gel Processing*. 1990, Academic Press Inc.

36. Rahaman, M., *Ceramic Processing and Sintering*: 1999, Marcel Dekker Inc.

37. Haneda, M., Kintaichi, Y., *Selective reduction over Ga_2O_3-Al_2O_3: effect of sol-gel method,* Catalysis, 2000. **192**: pp. 137-148.

38. Yoldas, B.E., *Hydrolysis of aluminum alkoxide and bayerite conversion.* Applied Chemical Biotech., 1973. **23**: pp. 803.

39. Fathollahi, V., Amini, M., *Sol–gel preparation of highly oriented gallium-doped zinc oxide thin films,* Materials Letters, 2001. **50**: pp. 235-239.

40. Bae, J., *Development of Nanostructured Alumina Sol-Gel Coating on CoCr Biomedical Alloy*. 2004, PhD thesis, UNSW.

41. Haneda, M., Kintaichi, Y., *Selective reduction of NO with propene over Ga_2O_3–Al_2O_3: effect of sol–gel method on the catalytic performance.* Journal of Catalysis. 2000. **192**: pp. 137–148.

42. Niederberger, M., Pinna, N., *Metal Oxide Nanoparticles in Organic Solvents*. 2009: Springer, New York.

43. Eldik, R., *Advances in Inorganic Chemistry*. Vol. 60. 2008: Elsevier Inc. Amsterdam.

44. Mitzi, D., *Solution Processsing of Inorganic Materials*. 2009: Wiley, New York.

45. Flynn, A., *Inorganic Chemistry*. 2009: Global Media, Horsham, West Sussex.

46. Ristic, M., Popovic, T., Music, S., *Application of sol–gel method in the synthesis of gallium(III)-oxide.* Materials Letters 2005. **59**: pp. 1227–1233.

47. Kokubun, Y., Miura, K., *Sol-gel prepared beta Ga_2O_3 thin films for ultraviolet photodetectors.* Applied Physics Letters, 2007. **90**: pp. 031912 (1/3).

48. Roy, R., Hill, V., Osborn, E., *Polymorphism of Ga_2O_3 and the system Ga_2O_3-H_2O.* J. Am. Cer. Soc., 1952. **71**: pp. 719-722.

49. Das, B., Roy, R., *Thermodynamics of the $GaCl_3$–HCl–H_2O system at 258°C.* Solution Chemistry, 2000. **29**: pp. 289-297.

50. Levin E., *Phase Diagrams for Ceramics*. The American Ceramic Society, 1964. pp. 321-323.

51. Schock, R., *Point Defects in Minerals*. Geophysical Monongraphs, 1985.**31**: pp. 232-245.

52. Unger, I., Mohamed, M., *The surface band structure of β-Ga_2O_3-software.* Journal of Physics: Conference Series, 2011. **286**: pp. 342-348.

53. Moulson, A., Herbert, J., *Electroceramics Materials, Properties, Applications*. 2003, John Wiley & Sons Ltd.

54. Buchanan, R., *Ceramic Materials for Electronics: processing, properties, and applications*. 1991, Marcel Dekker, Inc.

55. Hasnip, P., *A Beginner's Guide to Materials Studio and DFT Calculations with Castep*. 2007, York University, UK.

56. Segall, M., Lindan, P., *First-principles simulation: ideas, illustrations and the CASTEP code.* Condensed Matter, 2002. **14:** pp. 2717–2744.

57. Milman, V., Refson, K., *Electron and vibrational spectroscopies using DFT, plane w aves and ps eudopotentials: C ASTEP i mplementation.* Molecular Structure, 2010. **10**: pp. 1113-1114.

58. He, H., Orlando, R., *First-principles s tudy of t he s tructural, e lectronic, and optical p roperties o f Ga_2O_3-software.* Physical R eview B, 2006. **74**: pp. 1143-1148.

59. Ohira, S., Suzuki, N., *Characterization o f t ransparent an d c onducting Sn-doped β-Ga_2O_3 single crystal af ter anne aling-software.* Thin S olid F ilms, 2008. **516**: pp. 5763–5767.

60. Yamaga, M., *Donor st ructure a nd electric transport m echanism i n Ga_2O_3-software.* Physical Review B, 2003. **68**: pp.1157-1162.

61. Pauling, L., *The nature of t he c hemical bond and t he s tructure of m olecules and crystals*. 1960, Cornell University.

62. Zhu, Y., Zhang, L., *The c hemical s tates and pr operties of dope d TiO f ilm photocatalyst pr epared using t he Sol–Gel m ethod w ith TiCl as a p recursor.* Applied Surface Science, 2000. **158**: pp. 32–37.

63. Bai, S., T. T seng, *Effect of al umina dopi ng on s tructural, e lectrical, and optical p roperties of s puttered ZnO th in fi lms.* Thin S olid F ilms, 2006. **515**: pp. 872–875.

64. Patnaik, P., *Handbook of Inorganic Chemicals,* 2003, McGraw-Hill, Ne w York.

65. Bradley, S., Kydd, R., Yamdagni, R., *Detection of a ne w p olymeric species formed t hrough t he hydrolysis o f G allium(III) Sal t So lutions.* Chem. S oc., 1990. **2**: pp. 414-417.